quency U-shaped, flat, and high-frequency sloping. These data would suggest that the hearing impairment in our families is not a coincidence.

Preparation of DNA and RNA Samples

After informed consent was obtained, genomic DNA was extracted from peripheral-blood lymphocytes or lymphoblastoid cell lines by use of methods described elsewhere (Ishikawa et al. 1997). All families were excluded for SCA1, SCA2, SCA3/MJD, SCA6, SCA7, SCA8, SCA12, SCA14, SCA17, and DRPLA by testing mutations in the disease genes. For expression analysis on an RNA level, frozen cerebellar tissues of four brains affected with Alzheimer disease (AD) (age at death, range 65–85 years; duration of the disease, range 5–10 years) were used as controls. Clinically, these patients with AD showed a moderate-to-severe degree of dementia, as measured by the Clinical Dementia Rating (Hughes et al. 1982). Neuropathology in the cerebella of these patients showed only a few senile plaques without neuronal losses. For chromosome 16q22.1–linked ADCA, two patients were studied (ages at death, 74 and 78 years). Both control and 16q22.1-linked ADCA brains were obtained at autopsy, with the families' written consents approved by each institutional ethical committee. These brains were immediately frozen and stored at −80°C until use. Total RNA was extracted from frozen cerebellar tissues as described elsewhere (Ishikawa et al. 1999). Poly-A^+ RNA was selected from total RNA by NucleoTrap (Macherey-Nagel).

Restriction of Candidate Interval by Genotyping and Haplotype Analysis

Genotypes were determined for 23 informative markers, including five new markers we identified (*GGAA10, TTCC01, TA001, GA001,* and *AAT01* [GenBank accession numbers AB13610, AB13611, AB13612, AB1-97662, and AB13613, respectively]) (table 1). Standard PCR was performed in a final volume of 20 μl, containing 10 ng of genomic DNA, 3.4 pmol of each primer, 2.5 mM of dNTP, and 0.75 U of *Taq* polymerase (Takara). Thermal cycling was performed at 94°C for 5 min for initial denaturing, 30 cycles of denaturation (94°C for 30 s), annealing (55°C for 30 s), and extension (72°C for 30 s), followed by a final extension at 72°C for 5 min in an ABI GeneAmp PCR system 9700 (PE Applied Biosystems). The amplified product was separated in the Automated Laser Fluorescent DNA Sequencer II (Pharmacia Biotech), and genotypes were determined with Fragment Manager (Pharmacia Biotech) (Ishikawa et al. 1997). Allele frequencies in the general population were analyzed in 500 unrelated individuals without personal or family history of ataxia or other degenerative diseases.

Table 1

Microsatellite Markers and Primer Sequences

The table is available in its entirety in the online edition of *The American Journal of Human Genetics.*

Haplotypes of 16q22.1 markers were determined for 10 families (fig. 1) that were informative for determining the phase of alleles. The remaining 42 families were not sufficiently informative for determining the phase. Paucity of informative families was mainly due to the late age at onset of this disease. For these uninformative families, only combinations of genotypes were assessed, and the region of genotypes shared with the larger 10 families was compared.

Screening for Mutation in 21 Different Candidate Genes

Within the most critical interval, 21 genes or clusters of ESTs were retrieved from the Ensembl, UniGene, National Center for Biotechnology Information (NCBI), and Celera databases. Primers were designed to amplify individual exon and intron-exon boundaries for each gene, and genomic DNA was amplified by the aforementioned standard PCR protocol (primer sequences are available on request). Amplicons from controls and patients were first separated on 2% agarose gels, to determine by screening whether any aberrant bands were amplified from patient DNA samples. Residual solutions of PCR products were then purified with QIAquick PCR purification kit (Qiagen) and were directly sequenced using Applied Biosystems Model 377 or 3100 Automated Sequencer, as described elsewhere (Li et al. 2003). The mutation was analyzed by comparing sequenced data and annotated databases, with use of the software DNASIS (Hitachi). Genomic rearrangement was screened by Southern-blot analysis by use of cosmid clones for probe synthesis as described elsewhere (Kobayashi et al. 1998). In brief, cosmid clones, tandemly covering the chromosome 16q22.1–linked ADCA critical region, were generated by subcloning from the BAC contig (Li et al. 2003). Then, the radiolabeled (^{32}P) probe was generated from each cosmid clone. Genomic DNA extracted from lymphoblastoid cell lines of control individuals and patients with chromosome 16q22.1–linked ADCA was digested with a restriction enzyme and was subjected to Southern-blot analysis. To screen gene arrangement, analysis was performed with six different restriction enzymes (*Bam*HI, *Bgl*II, *Eco*RI, *Eco*RV, *Hind*III, and *Xba*I).

Twenty-one exons and 20 introns of the *puratrophin-1* gene, partially annotated as "*Q9H7K4,*" were sequenced entirely. The genomic region between the *puratrophin-1* gene and *SLC9A5* was also screened (fig. 2).

Families	P2	P4	P6	P12	P14	P15	T1	T2	T3	T4	T5	T6	T7	T8	T9	T10	T11	T12	T13	T14	T15	T16	T17
No. of patients	7	6	4	6	3	2	5	4	6	8	2	2	2	2	2	2	2	3	4	2	2	2	2
No. of at-risk individuals	12	1	2	2	7	2	3	3	3	4	4	0	0	0	0	0	2	2	0	0	1	0	0
DNA marker																							
D16S3031	9	9	9	9	9	9	9	9	10	9	10	1	10	3/9	9	9	9	9	8/9	9	9/10	9/10	9
GGAA05	1	6	1	1	1	1	1	2	5	1	1	1	2	1/2	1/2	1/6	1	1	1	1/4	2/4	1	1
GGAA10	3	3	3	3	3	3	3	3	4	3/5	3	3	3	3/4	3/5	3/4	3	3	3/5	3	3	3	3
TTCC01	6	6	6	6	6	5/6	6	6	6	6/7	6	6/7	6	6	6	6	6	6/7	6	6	5/6	6	6
D16S3086	2	2	2	2	2	2	2	2	2	2	2	2	2	2	2	2	2	2/3	2	2/3	2	2	2
GATA01	2	2/3	2	2	2	1/2	2	2	2	3	3	3	2	2	2	2/3	2	2	2	2	2	1/2	2
D16S421	3	3	3	3	3	3	3	3	3	3	3	3	3	3/5	3	3	3	3	3	3	3	3	3
Q9H7K4 /exon 1	T	T	T	T	T	T/C	T	T	T	T	T	T/C	T/C	T/C	T/C	T/C	T/C	T/C	T/C	T/C	T/C	T/C	T/C
TA001	1	1	1	1	1	1	1	1	1	1	1	1	1	1/8	1	1	1	1	1	1	1	1	1
GA001	4	4	4	4	4	4	4	4	4	4	4	4/7	4/7	4/7	4/7	4/5	4	4	4	4/7	4/5	4	4/7
TTTA001	4	4	4	4	4	4	4	4	4	4	4	4	4	4	3/4	4	4	4	4	4	4	4	4
CATG003	4	4	4	4	4	4	4	4	4	4	4	4	4	4	4	4	4	4	4/5	4	4	4	4
17msm	2	2	2	2	2	2	2	2	2	2	2	2	2	2	2	2	2/3	5	2	2/4	2/3	2	2
D16S3107	7	7	7	7	7	7	7	7	7	7	6	7	7	6	7	4/7	7	7	7	7/11	7	5	7/8
D16S3085	2	2	2	2	2	2	2	2	2	2	2	2	2	2	2	2	2	2	2	2	2	2	2
ATT01	2	2	2	2	2	2	2	2	2	2	2/4	2	2	2/3	2	2	2	2	2	2	2	2	2/3
GGAA01	6	6	6	6	6	6	6	6	6	6	6	7	6	5/6	5	6	4/6	6	6	6	5/6	1/6	6
D16S3025	4	4	4	4	4	4	4	4	4	4	3/4	4	4	4	4	4	4	4	4	4	4	4	4
CTTT01	8	8	8	8	8	8	8	8	9/10	8	5	9	8	8/10	4/10	9/10	12	10	8	9	8	8	8
D16S496	5	5	5	5	5	5	5	5	5	5	5	5	5	5	5	1/5	5	5	5	5	5	5	5
D16S3141	3	3	3	3	3	3	3	3	3	3	3	3	3	3	3	3/6	4	3	3	3/6	3	3/4	3
D16S3067	5	5	5	5	5	5	5	5	5	5	5	5	5	5	5	5	5	5	5	5	5	5	5
GT01	6	6	6	6	6	6	1/6	6	6	6	7	6	6	3/6	2/6	4/6	5	4	6	4/6	3/6	6	6
D16S3095	2	3	1	1	1	1	2	2	1	1	2	3	2	1/3	1	1/2	1	1/2	1	1/2	2	1	1/3

Families	T18	T19	T20	T21	T22	T23	T24	T25	T26	T27	T28	T29	T30	T31	T32	T33	T34	T35	T36
No. of patients	1	1	1	1	1	1	1	1	1	1	1	1	1	1	1	1	1	1	1
No. of at-risk individuals	0	0	0	0	0	0	0	0	0	0	0	0	0	0	0	0	0	0	0
DNA marker																			
D16S3031	9	9	9/10	9	9	9	9	9	9	9	1/9	9	9	8/9	8/9	1/9	9	9	8/9
GGAA05	1/5	1/3	1/4	1/5	1/5	1/2	1/5	5	1/2	1/5	1/7	1/5	1/5	1/5	2/5	1/4	1/4	1/5	1/3
GGAA10	2/3	3/6	3/6	2/3	3/5	3/4	1/3	2/4	3/7	3/6	3/5	1/3	3/8	3	3	3/4	3/4	3/5	3/5
TTCC01	6	6	6	6	6	6	6	6	6/7	6/7	6/7	6	5/6	4/6	6	6/7	6	5/6	6/7
D16S3086	2	2	2	2	2	2	2	2	2/3	2/3	2/3	2	2/3	2/3	2	2/4	2	2/3	2/3
GATA01	2	2/3	2	1/3	2	2	2/3	3/4	1/3	2	1/3	2	1	1/2	2/4	2/3	2	2	2
D16S421	3	3	3/4	3	3	3	3/4	3	3	3	3	3/4	3	3	3	3	3	3	3
Q9H7K4 /exon 1	T/C	T/C	T/C	T/C	T/C	T/C	T/C	T/C	T/C	T/C	T/C	T/C	T/C	T/C	T/C	T/C	T/C	T/C	T/C
TA001	1	1/9	1/10	1/7	1/8	1/7	1/6	2/8	1/6	1/10	1/10	1/7	1/9	1/9	1/8	1/16	1/9	1/7	1/5
GA001	4/7	1/4	4/7	4/8	4/7	4/5	4/7	4/5	4/7	4/7	4/7	4/7	4/6	4/8	4/5	4/7	4/8	4/7	4/6
TTTA001	4	4	4	3/4	3/4	3/4	3/4	4	4	3/4	4	4	3/4	4	3/4	4	4	4	1/4
CATG003	4	4	2/4	1/4	4	4/7	4	4/5	4	1/4	4	4/5	4	4	4	4	4	2/4	4
17msm	2	2/5	2/4	2/5	2/4	2/5	2/3	2/4	2/4	2/5	2/4	2/4	2/4	2	2/3	2/6	1/2	2	2/4
D16S3107	7	6	7	5/6	5/7	4/7	7	3/7	6/10	6/7	6	7	7	6/7	6/7	5/7	7/11	7/10	2
D16S3085	2	2	2	2	2	2	2	2	2	2/4	2	2/3	2	2/3	2	2	2/3	2/3	2
ATT01	2/6	2/3	2/3	2	2/3	2	2	2/3	2	2	2	2/4	2	2/3	2/4	2	2/3	2/3	2/4
GGAA01	4/6	3/6	6	2/6	4/6	6	4/6	2/6	4/6	5/6	6/7	6	6	4/6	6	5/6	3/6	2/6	3/6
D16S3025	4	4	4	4	4	4	4/6	4	4	4	4/5	4	4	4/5	4/5	4	4	4	4
CTTT01	9/10	9/10	5/10	3/9	8	9/10	10	9/10	8/10	8	8	7/8	8/11	7/9	8/9	3/9	9	5/9	4/8
D16S496	5	5	5/6	5	5/8	5/6	5	3/5	5	5	5	5	5	5	5	5	5	5	5
D16S3141	3/12	3	3	3/8	3/6	3/6	3/5	5	3	3/5	3/8	3	3	3/5	3/5	3	4/6	3/4	3
D16S3067	5	5	5	5	5	5	5	5	5	5	5	5	5	5	5	5	5	5	5
GT01	1/6	2/6	6	1/6	6/7	6	2/6	4/6	4/6	4/6	2/6	4/6	5/6	6	1/6	4/6	6	2/6	4/6
D16S3095	1	1	2	1/2	1/2	1/3	1/2	1/2	1/2	1/2	1/3	1/3	1	1/2	1/2	1/2	1/3	1/2	1

Families	T37	T38	T39	T40	T41	T42	T43	T44	T45	T46	Allele frequency (%)	Linkage disequilibrium (*P* value)
No. of patients	1	1	1	1	1	1	1	1	1	1		
No. of at-risk individuals	0	0	0	0	0	0	0	0	0	0		
DNA marker												
D16S3031	9	9	9/10	8/9	9	9	9	9	9	9	68.1	
GGAA05	1/3	1/4	1/6	1/2	1/5	1/3	1/5	2/4	1/4	2/6	1.4	
GGAA10	4/6	3/4	3	3/5	3/6	3	3/6	3/5	3/5	3/7	13.2	
TTCC01	5/6	6	5/6	6	6/7	6	5/6	5/6	6/7	5/6	60.5	
D16S3086	2/3	2	2/5	2	2	2	2/3	2	2	2	65.7	
GATA01	2	2	2	2/3	2	3	1/3	2/3	2	2/3	44.1	
D16S421	3	3	3	3	3/5	3/4	3	3	3	3	75.7	<.0001*
Q9H7K4 /exon 1	T/C	T/C	T/C	T/C	T/C	T/C	T/C	T/C	T/C	T/C	0	<.0001*
TA001	1/9	1/10	1/9	1	1/10	1	1/9	1/9	1/6	1/5	23.8	<.0001*
GA001	4/11	4/5	4/8	4/5	4/7	4/5	4/7	4/5	4/7	4/7	0.1	<.0001*
TTTA001	4	3/4	3/4	4	1/4	4	4	4	4	3/4	65	<.0001*
CATG003	4	4	4	4	4/6	4	4	4	4	4	76.9	<.0001*
17msm	2/5	2/3	2/5	2/4	2/10	2/4	2/4	4/6	2/4	2/4	8.3	
D16S3107	5/7	3/7	5/7	4/7	5/7	3/7	6/7	4/7	5/7	6/7	13.9	
D16S3085	2/4	2	2	2	2	2	2	2	2	2	81.8	
ATT01	2/3	2/4	2/5	2	2/3	2	2	2	2	2	47.5	
GGAA01	6	6/7	6/9	6/7	3/6	6	6/7	6/7	5/6	5/6	18.8	
D16S3025	4	4	4/5	4	4	4/5	4	4/6	4	4	75	
CTTT01	6/9	8/14	8/10	7/9	8/10	8/15	9/10	1/7	7/9	3/8	28.2	
D16S496	5	5	5	5	5	5	5	5	5	5	54.2	
D16S3141	3	3/5	3/5	3/4	3	3	3	3/5	3/6	3/7	44.4	
D16S3067	5	5	5	5	5	5	5	5	5	5	41.9	
GT01	4/6	4/6	5/6	5/6	6/7	6	3/6	3/4	4/6	4/6	15.8	
D16S3095	1	2/3	1/3	1/3	1/4	1/2	1/3	2	1/2	1	-	

Figure 1 Haplotype analysis in the chromosome 16q22.1–linked ADCA critical locus. Ten families (P2, P4, P6, P12, P14, and T1–T5) large enough for haplotype analysis are indicated (*yellow boxes at top*). A founder haplotype "3-1-4-4-4" was seen in all patients for markers 16cen-*D16S421-TA001-GA001-TTTA001-CATG003*-16qter, between *GATA01* and *17msm*. Two alleles are shown (separated by a virgule [/]) for cases in which phase could not be determined. An asterisk (*) indicates that *P* values show significant linkage disequilibrium by Fisher's exact probability test. The specific C→T change in the *puratrophin-1* gene lies within the founder chromosomal region.

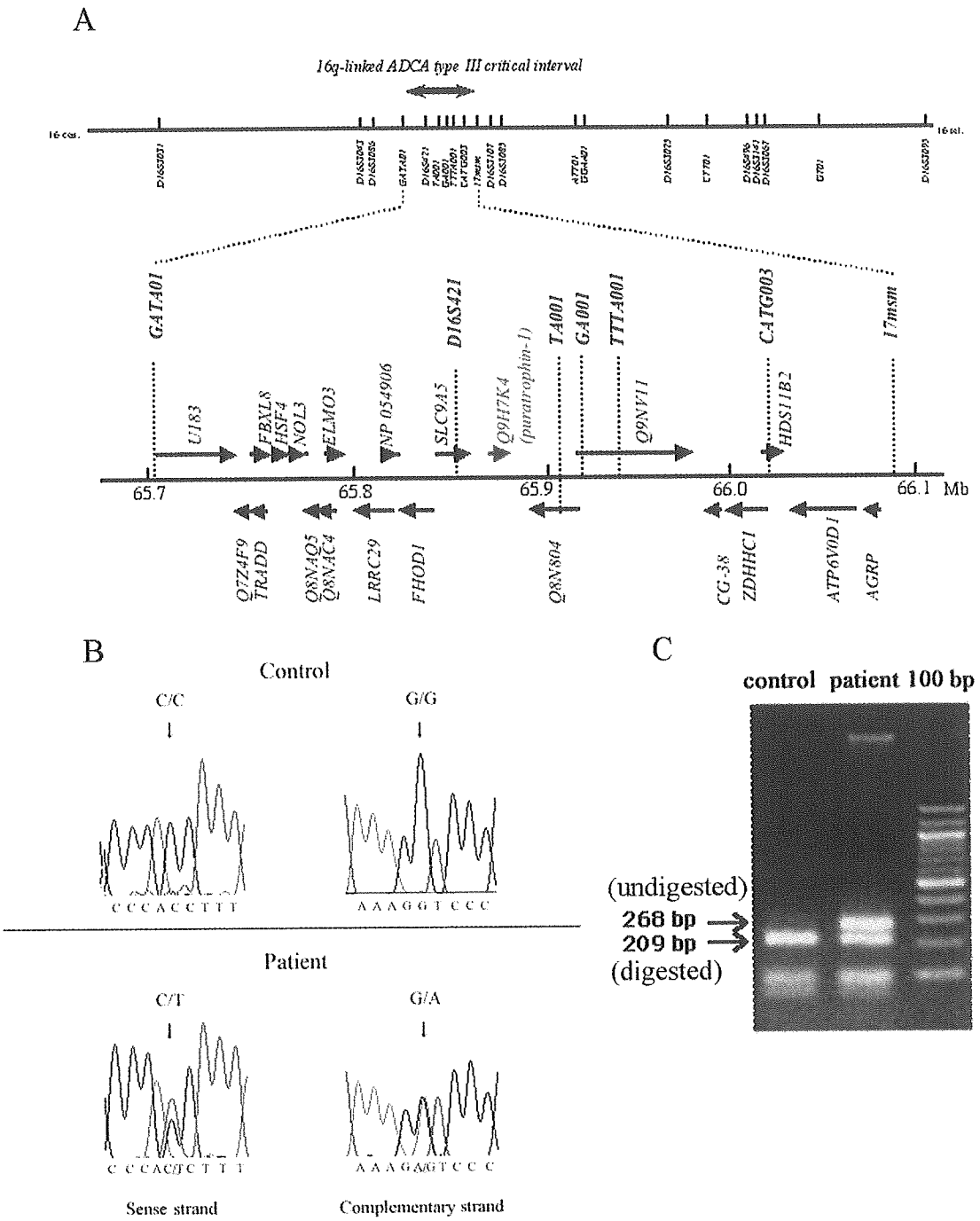

Figure 2 Positional cloning of the chromosome 16q22.1–linked ADCA gene. *A*, Genetic and physical maps of the interval in chromosome 16q22.1, showing microsatellite markers used to refine the interval. Twenty-one genes and their direction of transcription (Ensembl) are shown. *B*, Nucleotide sequences of exon 1 flanking the C→T single-nucleotide change in control and patient DNA samples. The patient harbors a heterozygous C→T substitution on the sense strand. *C*, RFLP by digestion with *Eco*NI. PCR was performed with primers UK1-E1F1 and UK1-E1R1. Whereas the normal allele produces digested fragments of 209, 92, and 59 bp, the C→T change in the mutant allele disrupts one *Eco*NI site, producing fragments of 268 and 92 bp.

The C→T change in the 5′ UTR was detected by amplifying genomic DNA with forward primer UK1-E1F1 (5′-CAGCGCGGTTCACACTGAGA-3′) and reverse primer UK1-E1R1 (5′-GGCCCTTTCTGACAGGACTGA-3′), which yielded a specific product of 360 bp. This amplicon harbors two *Eco*NI sites, one of which is destroyed by the C→T change.

Expression Analysis of Puratrophin-1 *mRNA by RT-PCR*

To characterize *puratrophin-1* mRNA in the human brain, poly-A$^+$RNA obtained from control human cerebellar tissues was reverse transcribed with SuperScript II (Stratagene), and the entire coding region was amplified with primers UKI-RT-025F (5′-TTCGCCTGCATTGCCCACTGAG-3′) and UK1-RT-005R (5′-CACACACATCAGAAAGGGTAGTCAAC-3′), which yielded a major product of 3,835 bp. To analyze alternative transcription, the PCR products were subcloned into pCR2.1-TOPO (Invitrogen), and 10 randomly selected clones from each brain mRNA (2 AD and 2 chromosome 16q22.1–linked ADCA cerebella) were sequenced and compared with partially annotated sequences (*Q9H7K4*, NCBI accession numbers BC054486 and AK024475). Rapid cloning of the 5′ and 3′ ends (5′- and 3′-RACE) was performed using Marathon-ready cDNA kit (Clontech [BD Biosciences]) as described elsewhere (Tsunemi et al. 2002). The entire 5′ UTR was amplified with primers UK1-RT-493F (5′-TGAGACAGTCTCAGTCAGGTCAC-3′) and UK1-RT-021R (5′-GTGGGCACACAGAAGCAGCACTGC-3′), was subcloned into pCR2.1-TOPO (Invitrogen), and was sequenced.

Expression of the *puratrophin-1* gene in various human tissues was studied by RT-PCR with use of primers UKI-RT-025F and UK1-RT-005R on human Multiple Tissue Panels I and II (Clontech [BD Bioscience]). Expression levels of *puratrophin-1* mRNA were compared among control and patient cerebellar cortices by RT-PCR with use of primers UK1-RT-BF001F (5′-TCACGGTTCCCCGCGGCTCG-3′) and UK1-RT-BF019R (5′-GGTTGCATGGCCCTGAGAGTCTGG-3′), which yielded PCR products of 291, 419, and 505 bp, depending on alternative transcription. To compare *puratrophin-1* mRNA levels more precisely, real-time RT-PCR analysis was performed on four control (individuals with AD) and two chromosome 16q22.1–linked ADCA cerebella by use of TaqMan technique (Applied Biosystems) on Applied Biosystems 7700 Sequence Detection System. PCR was performed for total *puratrophin-1* mRNAs (i.e., full-length and short-form mRNAs [GenBank accession numbers AB197663 and AB197664, respectively]; definitions of these two isoforms are described in the "Results" section) with primers total-taq-F (5′-TGGAGAGATGAGTGTCAAGACTTTG-3′) and total-taq-R (5′-AATGACTTGGGTCTGCCTTGG-3′). The short-form *puratrophin-1* mRNA was specifically assessed with primers short-taq-F (5′-ATGCCACCGACTGGAGATTT-3′) and short-taq-R (5′-GCTGCCCTGTAGCTCCTCAT-3′). The TaqMan probe for total *puratrophin-1* mRNA was 5′-FAM-CCAGATGCACGTTAAGGACCCAGGTC-TAMRA-3′, and that for short-form *puratrophin-1* mRNA was 5′-FAM-TCTCTGACCCTACTCAGGCTGAAGCCC-TAMRA-3′. The experiments were performed three times and were averaged. The level of *puratrophin-1* mRNA was assessed relative to the level of *G3PDH* mRNA amplified with primers supplied from the manufacturer (Applied Biosystems). Since the expression level of *G3PDH* mRNA was >1,000-fold higher than that of *puratrophin-1* mRNA, one control individual was chosen and the value of *puratrophin-1* mRNA:*G3PDH* mRNA ratio (designated "*puratrophin-1* mRNA/*G3PDH* mRNA index") was standardized as "1"; another three control individuals and two patients were compared relatively. The difference between the control and patient groups was statistically analyzed with the Mann-Whitney *U* test.

To see the effect of the C→T change in the 5′ UTR of *puratrophin-1* gene on expression in vitro, the partial 5′-UTR fragment containing the mutation site was amplified with forward primers UK1-UF10-F2 (5′-CCGGAATTCCAGGCCTGAATTGCAGTTC-3′) and UK1-UF10-R2 (5′-CCAGGCATCCCTGAAACT-3′) and was subcloned into the *Hind*III-*Nco*I sites of the luciferase assay vector, pGL3-Control Vector (Promega). The C→T mutation was then generated by site-directed mutagenesis (Stratagene). Three types of vectors (mock, empty pGL3-Control Vector; wild-type, pGL3 with normal *puratrophin-1* 5′ UTR with allele C; and mutant, pGL3 with mutant *puratrophin-1* 5′ UTR with allele T) were separately transfected with Renilla vector (Promega) into HEK293 cells to equalize the transfection efficiency. The transfection experiment was performed independently three times. Luciferase activity (F/R: fire-fly luciferase activity against Renilla activity) was assayed in accordance with the manufacturer's protocol and was statistically analyzed with the Mann-Whitney *U* test.

Generation of Rabbit Polyclonal Antibodies against Puratrophin-1

On the basis of the deduced amino acid sequence of "full-length" and "short-form" puratrophin-1, the secondary structure of each isoform was predicted, and five synthetic peptides were designed: polypeptide *FL01* (aa 1–13), N-MERPLENGDESPD-C; *FL02* (aa 421–432), N-MDKADELYDRVD-C; *FL03* (aa 570–583), N-EEGQRVLAELEQER-C; *FL04* (aa 991–1003), N-RFEIWFRRRKARD-C; and *SV01* (aa 13–26), N-REVWEGNGDAWRDE-C. The polypeptide FL01 lies at the amino terminus of the puratrophin-1 (fig. 3). Therefore, the

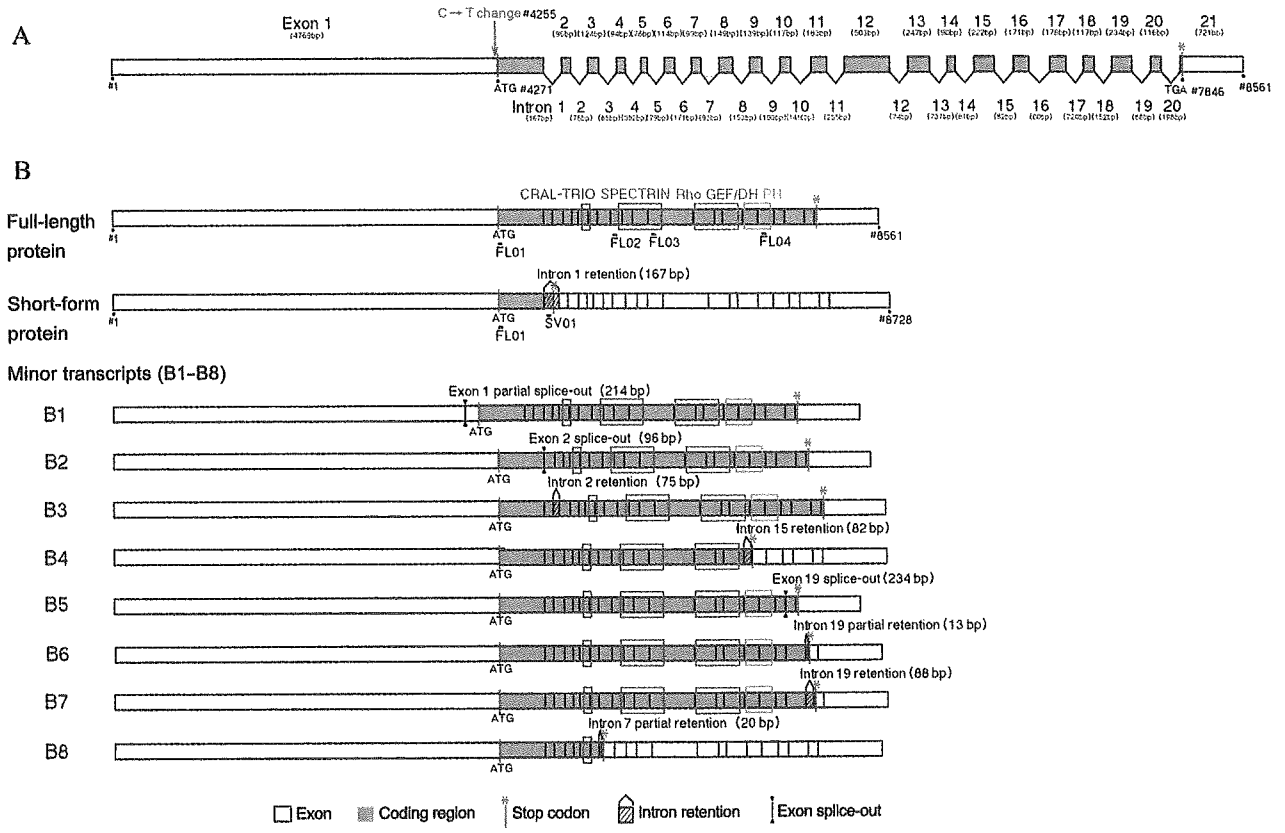

Figure 3 Genomic and mRNA structure of the *puratrophin-1* gene. *A*, Intron-exon structure of *puratrophin-1*. Exons are shown as vertical bars, and coding regions are shown in red. The C→T change at nt 4255 (or, 16 nt upstream of the translation initiation codon) is indicated. Nucleotide numbers (indicated by a number sign [#]) are counted from the 5′ end. *B*, *Puratrophin-1* mRNAs cloned from the human cerebellum. Major transcripts are full-length and short-form *puratrophin-1* mRNAs; minor transcripts (B1–B8) were also cloned. The CRL-TRIO, spectrin, Rho GEF/DH, and PH domains are indicated. Epitopes for five rabbit anti–puratrophin-1 antibodies (FL01–FL04 and SV01) are also mapped. Antibodies FL02, FL03, and FL04 are designed to specifically detect full-length puratrophin-1, the antibody SV01 specifically detects short-form puratrophin-1, and the antibody FL01 detects both full-length and short-form puratrophin-1.

antibody Prtrphn1-Ab FL01 would detect both full-length and short-form puratrophin-1. The polypeptides FL02, FL03, and FL04 are specific for the full-length puratrophin-1 (fig. 3). Notably, FL03 is at the spectrin repeat motif. The polypeptide SV01 lies at the carboxyl-terminus of the short-form puratrophin-1. Therefore, the antibody Prtrphn1-Ab SV01 would specifically recognize the short-form puratrophin-1. Each antigen was immunized into rabbit, and polyclonal antibodies were obtained as described elsewhere (Ishikawa et al. 1999).

The specificity of Prtrhn1-Abs was assessed by detection of recombinant puratrophin-1 protein. For this purpose, an antisense-strand primer was designed to encode hemagglutinin A (HA) in-frame at the carboxyl-terminus of the puratrophin-1. By PCR, full-length *puratrophin-1* cDNA with the HA-coding nucleotide sequence at its 3′ end was generated and was then cloned into pcDNA1 expression vector (Invitrogen). The puratrophin-1–HA fusion protein, transiently expressed in HEK293 cells, was first immunoprecipitated with Prtrhn1-Abs and then was detected with rat monoclonal anti-HA High Affinity antibody (3F10 [Roche Mannheim]) (fig. 4). The fusion protein immunoprecipitated with preimmune sera was not detected with anti-HA antibody.

Specificity of Prtrphn1-Abs on immunohistochemistry was assessed by immunoabsorption test. Solutions containing Prtrphn1-Ab and different concentrations of antigen (synthetic peptide) (0, 0.01, 0.1, and 1 mg/

The figure is available in its entirety in the online edition of *The American Journal of Human Genetics*.

Figure 4 Immunoprecipitation of puratrophin-1–HA fusion protein and immunoabsorption test with antiserum against puratrophin-1. The legend is available in its entirety in the online edition of *The American Journal of Human Genetics*.

liter) were made. Sections were incubated overnight with these solutions as other immunohistochemical staining. Prtrphn1-Abs were completely absorbed by peptides of higher concentrations (fig. 4).

Immunohistochemical Analyses of Puratrophin-1, Golgi-Apparatus Protein G58K, and Spectrin in Control Mouse, Human, and 16q22.1-Linked ADCA Tissues

Five polyclonal antibodies against puratrophin-1 (Prtrphn1-Ab types *FL01*, *FL02*, *FL03*, *FL04*, and *SV01*) were used for immunohistochemistry. Mouse monoclonal antibody against the microtubule-binding peripheral Golgi-apparatus membrane protein G58K (Sigma) and the mouse monoclonal antibody for α- and β-spectrin (MAB372 [Chemicon International]) were also used for immunohistochemistry.

Formalin-fixed paraffin-embedded tissue sections were prepared. Examined tissues were C57BL/6J wild-type mouse tissue, including cochlea (1 d postnatal), normal-control human tissues (testis, pancreas, prostate gland, lung, liver, heart, kidney, and brain from three individuals who died with nonneurological diseases), disease-control human brains (AD [n = 3], SCA6 [n = 2], multiple-system atrophy [MSA] [n = 3], and SCA3/MJD [n = 3]), and three brains with chromosome 16q22.1–linked ADCA. Immunohistochemistry was performed as described elsewhere (Ishikawa et al. 1999). In brief, sections were incubated overnight with Prtrphn1-Abs (diluted 1:200 with PBS), G58K (diluted 1:400), or MAB372 (diluted 1:200) at 4°C, after which the primary antibody was serially detected with avidin-biotinylated peroxidase complex method (Vector), was developed with 3,3′-diaminobenzidine (DAB), and was counterstained with hematoxylin.

Results

Restriction of the Critical Interval to <600 kb within Human Chromosome 16q22.1

Haplotype reconstruction of 10 informative families revealed that all affected individuals in these families were segregated with the haplotype 3-1-4-4-4 for markers *16cen-D16S421-TA001-GA001-TTTA001-CATG003-16qter* lying between *GATA01* and *17msm* (fig. 1). Genotypes of all affected individuals in the remaining 42 families that were not informative enough for haplotype reconstruction were also consistent with the common haplotype. Particularly, a dinucleotide (GA) repeat marker *GA001* showed strong linkage disequilibrium: the allele 4 of GA001 was seen in all affected individuals in all families with chromosome 16q22.1–linked ADCA, whereas that allele was seen very rarely (frequency 0.1%) in 1,000 control chromosomes (fig. 1). Whereas only one common haplotype was seen between *GATA01* and *17msm*, different alleles were seen for *GATA01* and other centromeric markers or for *17msm* and other telomeric markers (fig. 1). These results indicate that the gene for chromosome 16q22.1–linked ADCA is most likely to exist in the interval between *GATA01* and *17msm*. This region was within the previously refined intervals (Hellenbroich et al. 2003; Li et al. 2003) and was considered to be <600 kb in size in the database Ensembl.

Identification of a Single-Nucleotide Substitution in the 5′ UTR of the Gene Encoding Puratrophin-1 in the Critical Interval

Within the critical interval between *GATA01* and *17msm*, 21 different genes were identified (fig. 2*A*). We screened all 21 genes by direct sequencing of amplified genomic PCR products of all coding exons and flanking intronic sequences. Genomic Southern-blot analyses were also performed but did not detect any rearrangement (fig. 5).

We found that all patients with chromosome 16q22.1–linked ADCA harbored a heterozygous C→T single-nucleotide substitution at the position 16 nt upstream of the putative translation initiation codon of the gene *Q9H7K4*, encoding hypothetical protein DKFZP434I216 (NCBI accession number BC054486) (fig. 2*B*). All the at-risk individuals who had the founder haplotype between *GATA01* and *17msm* also harbored the C→T change. The ages of these individuals were below the maximum age at disease onset in their families, which indicates that they could be in presymptomatic stages. On the other hand, this C→T substitution was not seen in 500 healthy Japanese individuals (1,000 chromosomes), confirmed by *Eco*NI RFLP analysis (fig. 2*C*). All intronic sequences between the 21 exons and all the 8-kb sequences upstream of the *Q9H7K4* gene were also directly sequenced. Although there was a G→A SNP 44 nt upstream of the 3′ splice site of intron 9 of the *Q9H7K4* gene, the allele segregating with the disease was also seen in 75% of control chromosomes. As far as we examined, the C→T change at the position 16 nt upstream of the putative translation initiation codon of the gene *Q9H7K4* was the only specific change seen for patients with chromosome 16q22.1–linked ADCA. We renamed this protein "puratrophin-1," meaning Purkinje cell atrophy associated

The figure is available in its entirety in the online edition of *The American Journal of Human Genetics.*

Figure 5 Southern-blot analysis. The legend is available in its entirety in the online edition of *The American Journal of Human Genetics.*

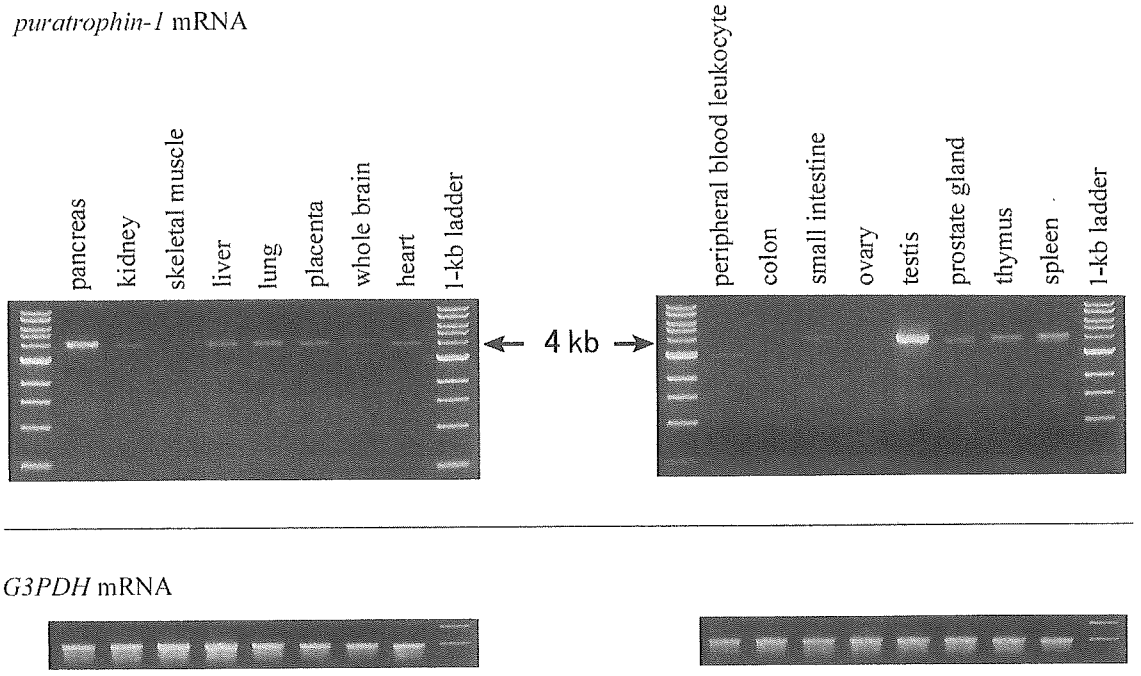

Figure 6 *Puratrophin-1* mRNA expression in various control human tissues. With this nonquantitative RT-PCR analysis, a relatively stronger expression was observed in the testis and pancreas, whereas mild or moderate expression was seen in the spleen, thymus, prostate gland, heart, placenta, lung, liver, and kidney. *Puratrophin-1* mRNA expression was low in the ovary, small intestine, colon, peripheral-blood leukocytes, whole brain, and skeletal muscle.

protein-1. (We reserved the nomenclature "ataxin-4" for families with original SCA4.)

Characterization of the Puratrophin-1 *Gene and Its Expression*

The *puratrophin-1* gene comprises 20 introns and 21 exons spanning a 13.7-kb genomic region (fig. 3*A*). RT-PCR and RACE experiments revealed that this gene is expressed in the human brain with an 8,561-nt mRNA and a single ORF of 3,576 nt (from nt 4,271 to nt 7,846) (fig. 3*B*). The first exon was 4,769 nt in length. This "full-length" transcript is predicted to encode a 134-kD protein, consisting of 1,192 aa, that contains four important domains: the cellular retinaldehyde-binding (CRAL)/triple function domain (TRIO) (at codons 304–338), the spectrin-repeat domain in the middle portion (at codons 447–601), the guanine-nucleotide exchange factor (GEF) for Rho/Rac/Cdc42-like GTPases followed by the Dbl-homologous (Rho GEF/DH) domain (at codons 733–907), and the pleckstrin-like homology (PH) domain (at codons 921–1027). The presence of these four domains suggests the role of puratrophin-1 in intracellular signaling and actin dynamics targeted to the Golgi apparatus (Godi et al. 1998; Fucini et al. 2000).

Besides the full-length *puratrophin-1* mRNA, we also found several alternative transcripts in human cerebellar cDNA (fig. 3*B*). The most common one had an unspliced intron 1 between exons 1 and 2 ("short-form" *puratrophin-1* mRNA). This intron retention produced a frameshift after exon 1 that resulted in a premature stop codon after 26 aa residues in intron 1. There were several other alternative transcripts (B1–B8 [fig. 3*B*]) in addition to full-length and short-form *puratrophin-1* mRNA. However, expression levels of these transcripts were considered lower than those of full-length or short-form *puratrophin-1* mRNA, as judged from cloning frequencies. *Puratrophin-1* mRNA was expressed in many tissues with various expression levels (fig. 6). The strongest expression was observed in the testis and pancreas, whereas its expression level was low in the "whole" brain. The expression was very weak on northern-blot analysis, even in the testis and pancreas (data available on request), which indicates that the expression of *puratrophin-1* mRNA was not abundant.

The Consequence of a C→T Change for Puratrophin-1 *mRNA Expression*

The consequence of the C→T change in the *puratrophin-1* gene was assessed by RT-PCR on frozen cerebellar tissues of two patients. No aberrant *puratrophin-1* mRNA was detected, which indicates that the mutation in the 5′ UTR does not affect alternative transcrip-

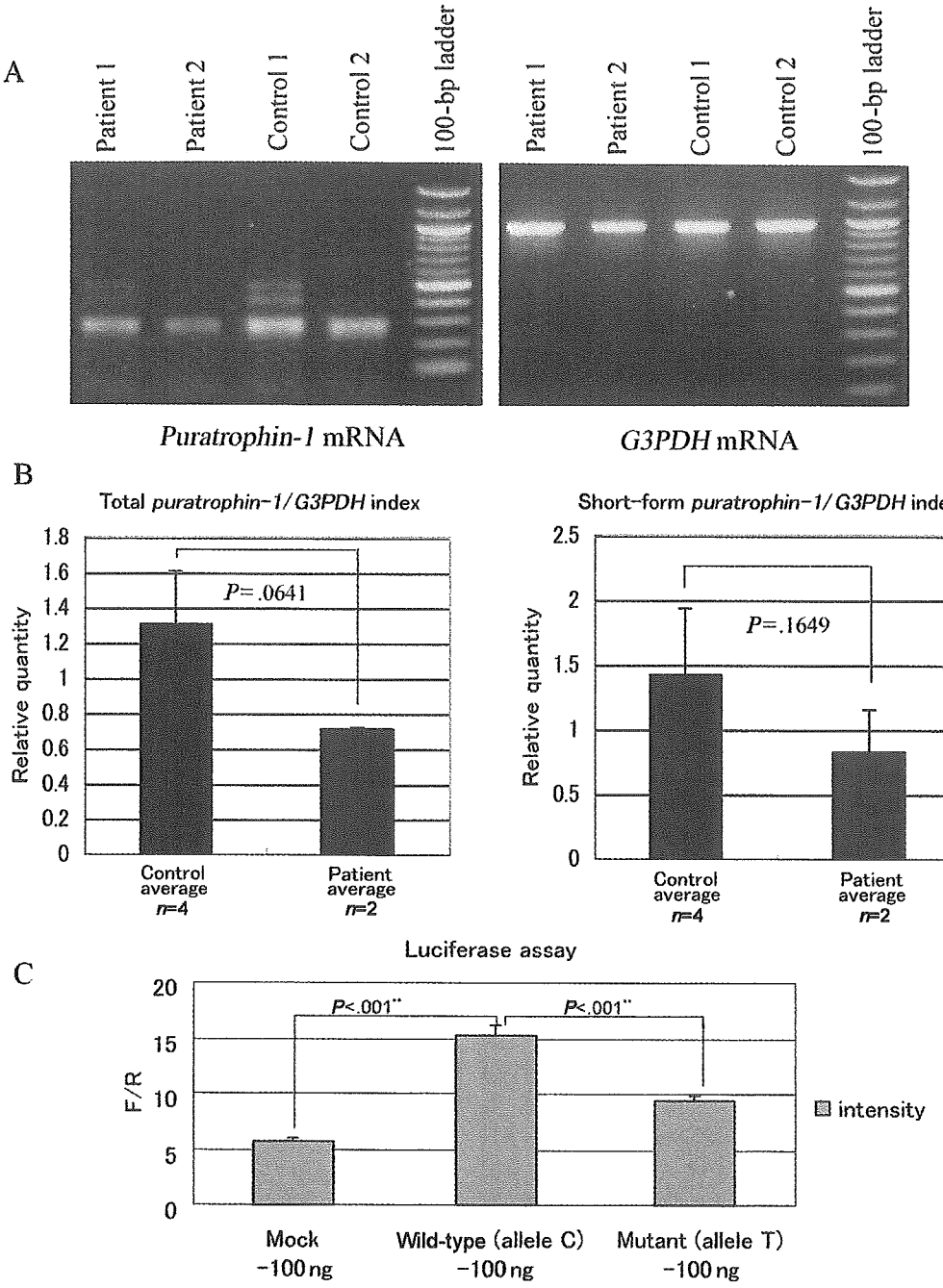

Figure 7 The consequence of a C→T change in the 5′ UTR of *puratrophin-1* mRNA. *A*, The *puratrophin-1* mRNA level assessed relative to *G3PDH* mRNA levels. The *puratrophin-1* mRNA levels in the cerebella of individuals with chromosome 16q22.1–linked ADCA appear slightly decreased compared with levels in control individuals. *B*, Quantitative analysis of *puratrophin-1* mRNA, with the use of the TaqMan technique in cerebellar mRNAs of four control individuals (with AD) and of two individuals with chromosome 16q22.1–linked ADCA. Both total *puratrophin-1* mRNA (i.e., full-length and short-form mRNAs) and short-form *puratrophin-1* mRNAs tended to be reduced in cerebella of individuals with chromosome 16q22.1–linked ADCA, although the significance was not statistically proven ($P = .0641$ for total mRNA; $P = .1649$ for short-form mRNA). C, Histogram of in vivo luciferase assay. "F/R" denotes fire-fly luciferase activity versus Renilla activity. The wild-type construct with allele C increases luciferase expression compared with an empty vector (Mock), whereas the mutant construct with allele T demonstrates significantly reduced luciferase activity ($P < .001$).

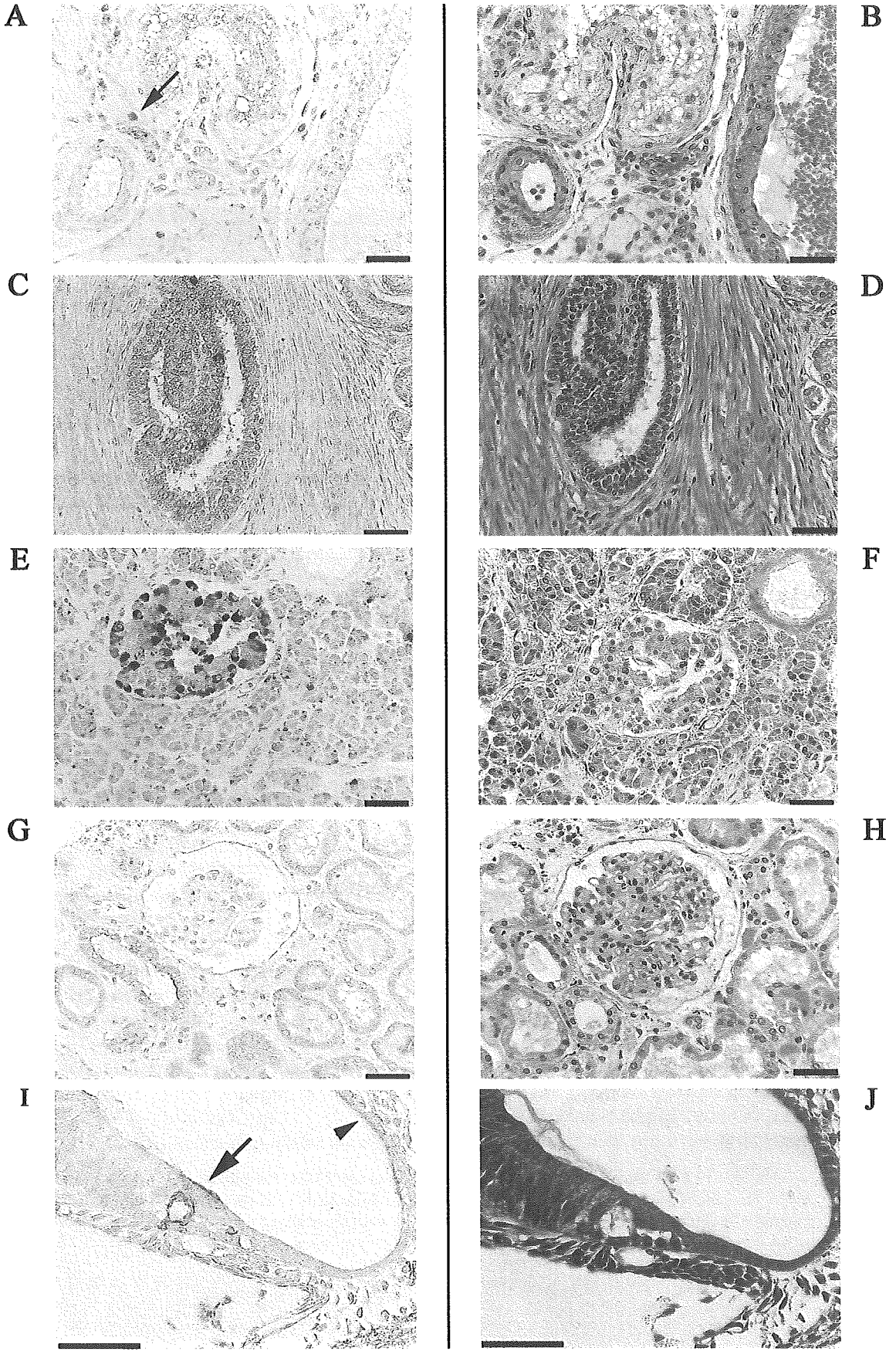
A
B
C
D
E
F
G
H
I
J

tion significantly. Instead, the expression level of *puratrophin-1* mRNA in the patient cerebella appeared slightly low compared with that in control cerebella (fig. 7*A*). On real-time RT-PCR analysis by TaqMan technique, the expression of *puratrophin-1* mRNA in the patient cerebella appeared lower than that in the control samples (fig. 7*B*). The tendency of reduction was seen for both total and short-form *puratrphin-1* mRNAs, although the significance was not proven statistically ($P = .0641$ for total *puratrophin-1* mRNA; $P = .1649$ for short-form *puratrophin-1* mRNA).

The in vitro study with *puratrophin-1* 5′-UTR sequences subcloned into luciferase expression vectors showed significantly reduced luciferase activity; the construct had mutant allele T, and the wild-type construct had allele C (fig. 7*C*). These data suggest that the C→T change in the *puratrophin-1* 5′ UTR could lead to reduced mRNA expression.

Expression of Puratrophin-1 in Control Human and Mouse Tissues and in Brains of Patients with 16q22.1–Linked ADCA

We next examined puratrophin-1 expression by immunohistochemistry using rabbit polyclonal Prtrhn1-Abs. Puratrophin-1 expression was seen in many control human tissues and mouse cochlea (fig. 8). Interestingly, puratrophin-1 expression was commonly seen in epithelial cells, such as epithelial cells in the human testis and hair cells in the mouse cochlea. As far as we examined in human tissues, the strength of immunoreactivity correlated with the mRNA expression level revealed by RT-PCR experiments (fig. 6).

In control human brains, both full-length and short-form puratrophin-1 was expressed faithfully in various neurons but most strongly in Purkinje cells (fig. 9*A*). In chromosome 16q22.1–linked ADCA brains, a striking difference was noted: the presence of microscopic aggregates of puratrophin-1 in the cytoplasm of Purkinje cells (fig. 9*B*). These aggregates were detected with all Prtrhn1-Abs, which indicates that full-length puratrophin-1 and short-form puratrophin-1 were both involved in the aggregate. On the other hand, puratrophin-1 aggregates were not obvious in neurons other than Purkinje cells. The finding of puratrophin-1 aggregates was specific to chromosome 16q22.1–linked ADCA brains, since the aggregates were not seen in other diseases showing degeneration of Purkinje cells, such as SCA6 or MSA.

We next examined the expression of G58K and of the α- and β-spectrin on control and chromosome 16q22.1–linked ADCA brains. Whereas G58K and spectrin were homogeneously stained in control brains (fig. 9*C* and 9*E*), these proteins both formed aggregation within the Purkinje cell of chromosome 16q22.1–linked ADCA brains (fig. 9*D* and 9*F*). This further suggests that formation of puratrophin-1 aggregates is abnormal and associates with disturbances of Golgi apparatus and spectrin.

Discussion

The single-nucleotide C→T substitution in the 5′ UTR of the *puratrophin-1* gene is strongly associated with chromosome 16q22.1–linked ADCA, as evidenced by the following three points. First, this single-nucleotide change was the only specific difference detected in patients, as far as we screened all exons and intron-exon boundaries of the 21 annotated genes lying within the founder chromosome. The change completely segregated with the disease in 52 unrelated families that originated in all sections of Japan, whereas such a change was not seen in 1,000 control chromosomes. We also screened for genomic rearrangement by Southern-blot analysis, but we did not observe any changes. Second, the C→T change was not a mere polymorphism present in the founder chromosome, since it resulted in reduced expression in the in vitro luciferase assay. Consistently, tendency for reduction in mRNA expression was seen in the cerebellum of chromosome 16q22.1–linked ADCA. Third, puratrophin-1 was aggregated in the major target neuron (i.e., the Purkinje cell) of chromosome 16q22.1–linked ADCA. The Golgi-apparatus membrane protein (G58K) and spectrin, both important cytoskeletal proteins, were also aggregated. Since aggregation of mutated protein is a common feature of many neurodegenerative disorders (Ross and Poirier 2004), a single-nucleotide change in the 5′ UTR in the *puratrophin-1* gene appears to be the mutation that causes chromosome 16q22.1–linked ADCA. Most mutations that cause ADCAs reside in genes encoding proteins whose functions are not well understood, except for the α1A-calcium channel ($Ca_v2.1$) for SCA6 (Zhuchenko et al. 1997), PKCγ for

Figure 8 Expression of puratrophin-1 in control human and mouse tissues. *A* and *B*, Human testis. *C* and *D*, Human prostate gland. *E* and *F*, Human pancreas. *G* and *H*, Human kidney. *I* and *J*, Mouse cochlea. *A*, *C*, *E*, *G*, and *I*, Immunohistochemical analysis with use of the polyclonal anti–puratrophin-1 antibody SV01. *B*, *D*, *F*, *H*, and *J*, Hematoxylin and eosin stain of the section adjacent to that shown in *A*, *C*, *E*, *G*, and *I*, respectively. Puratrophin-1 is expressed in many tissues, with varying strength. In particular, Leydig cells in the testis (*arrow* in *A*), epithelial cells in the prostate gland (*C*), and Langerhans islet in the pancreas (*E*) showed strong immunoreactivity. Immunoreactivity in the kidney was weak (*G*). Expression in the cochlea was particularly intense at the sensory hairlets (*arrow* in *I*). Hair cells of the stria vascularis also showed immunoreactivity (*arrowhead* in *I*). All scale bars = 50 μm.

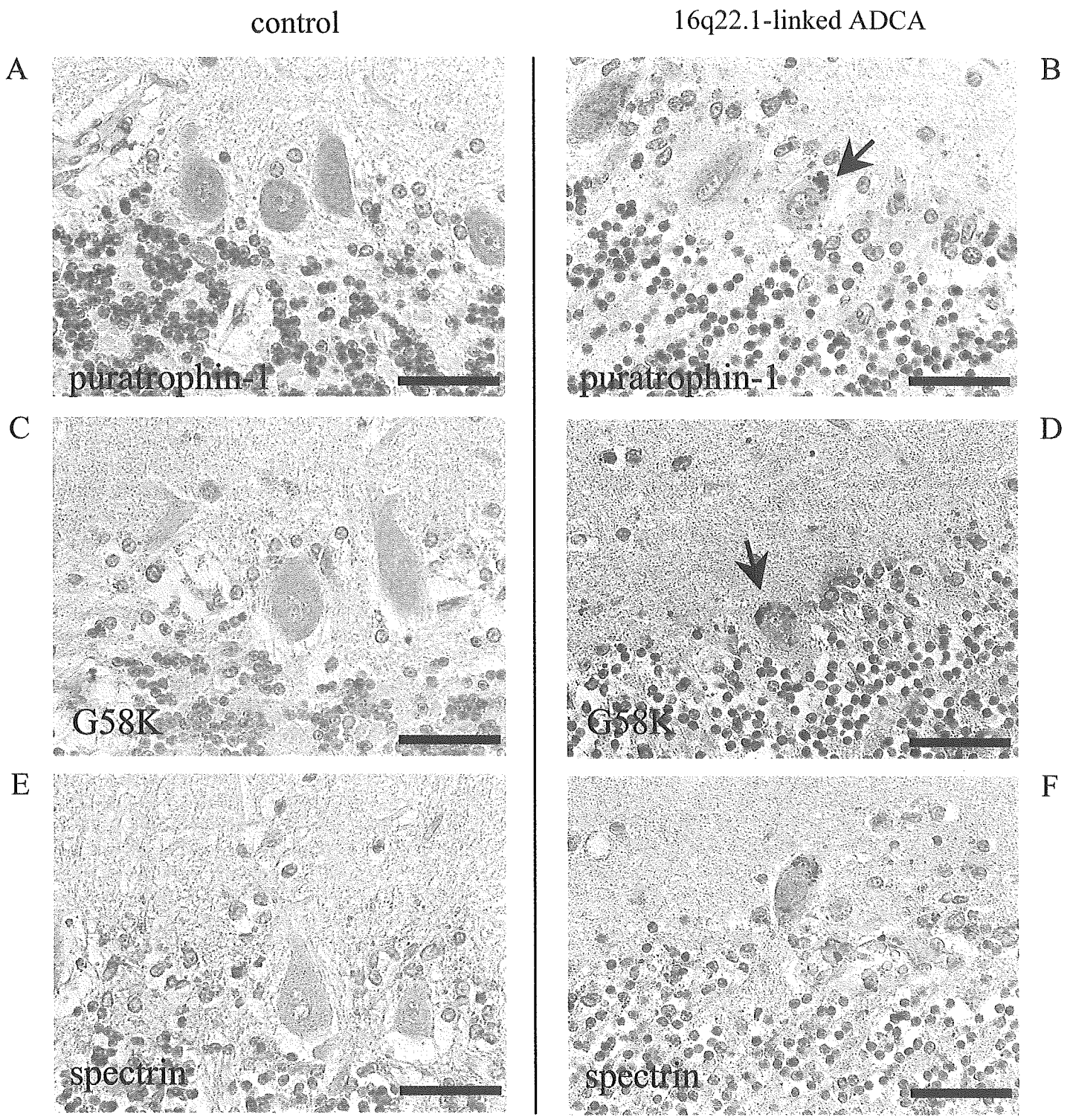

Figure 9 Immunohistochemical analysis of puratrophin-1, Golgi-apparatus membrane protein (G58K), and spectrin in control cells and samples from a patient's cerebellum. *A*, Puratrophin-1 expression in the cell body of Purkinje cells, visualized with use of rabbit polyclonal anti–puratrophin-1 antibody (FL01). *B*, With use of same antibody FL01, aggregation of puratrophin-1 (*arrow*), seen in a Purkinje cell of a brain affected with chromosome 16q22.1–linked ADCA. *C*, G58K expression, seen diffusely in the cell body of control Purkinje cells. *D*, G58K aggregation (*arrow*), morphologically quite similar to the puratrophin-1 aggregate, seen in a patient's Purkinje cell. *E*, Spectrin expression, seen in the cell body of a control Purkinje cell. *F*, Spectrin aggregation in a patient's Purkinje cell. All scale bars = 50 μm.

SCA14 (Chen et al. 2003), TATA-binding protein for SCA17 (Koide et al. 1999), and FGF14 for ADCA with FGF14 mutation (van Swieten et al. 2003). Puratrophin-1 is the first known protein related to intracellular signaling and cytoskeleton that is associated with ADCA. Our preliminary results suggest that the frequency of chromosome 16q22.1–linked ADCA is relatively high, since it was ranked the third most frequent ADCA in Japan, after MJD/SCA3 and SCA6. Since chromosome 16q22.1–linked ADCA had a strong founder effect, it will be important to clarify whether this specific C→T change is seen in other ethnic groups. Particularly, it is extremely important to clarify whether original patients with SCA4 reported from North American and German populations harbor mutation within the *puratrophin-1* gene (Flanigan et al. 1996; Hellenbroich et al. 2003).

A heterozygous, single-nucleotide substitution in the 5′ UTR that is associated with aggregation of the gene product is a unique feature as a cause of human disease. Generally, a single-nucleotide substitution in the 5′ UTR may result in expression of aberrant mRNA, abnormal trafficking of mutant transcripts due to conformational changes, or reduced transcription of mRNA, as in β thalassemia intermedia (Sgourou et al. 2004). In the present study, no aberrant transcripts were cloned from patient brains. Instead, the result from the in vitro study suggested that the transcription efficiency could be reduced significantly by the C→T substitution in the 5′ UTR of the *puratrophin-1* gene. Consistent with this in vitro finding, levels of *puratrophin-1* mRNA tended to be lower in cerebella of patients with 16q22.1-linked ADCA than in those of AD-affected controls. Further studies comprising a larger number of samples that include "neurologically normal" controls will be necessary to confirm that reduced *puratrophin-1* mRNA expression is associated with the C→T change in the 5′ UTR. Although aggregations of mutated proteins in most neurodegenerative diseases are due to conformational changes produced by amino acid alterations, reduced protein expression may also cause protein aggregation, such as the neurofilament light-chain aggregation in anterior horn cells of patients with amyotrophic lateral sclerosis (ALS) (Bergeron et al. 1994). It is currently not known how the C→T change in the *puratrophin-1* gene leads to puratrophin-1 aggregation. However, it is possible that alteration in the stoichiometry or changes in the protein stability, observed in neurofilament proteins in ALS (Ge et al. 2003), also exist for puratrophin-1 in chromosome 16q22.1–linked ADCA. In addition, it should be noted that since reduction of *puratrophin-1* mRNA levels in patient cerebella was small, that may not be a sufficient explanation of the formation of aggregation. It will be important to assess the *puratrophin-1* mRNA levels specifically in Purkinje cells, where the protein aggregates.

Puratrophin-1 is a novel protein with four important domains: the spectrin repeat, CRAL/TRIO, Rho GEF/DH, and PH domains. Therefore, the *puratrophin-1* gene would be the fifth gene that encodes Rho GEF protein to be associated with human disease, after the *FGD1GEF* gene for faciogenital dysplasia (Pasteris et al. 1994), the *ARHGEF6* gene for X-linked nonsyndromic mental retardation (Kutsche et al. 2000), the *ARHGEF10* gene for autosomal dominant neuropathy with thin myelinated fibers (Verhoeven et al. 2003), and the *ALS2* gene for the autosomal recessive juvenile motor neuron disease ALS2 (Hadano et al. 2001; Yang et al. 2001). GEFs exert diverse functions in intracellular-membrane trafficking and microtubule dynamics and ultimately regulate numerous cellular responses—such as proliferation, differentiation, and movement—by activating small G-protein GTPases (Rossman et al. 2005). Although Rho GEF/DH and PH domains are typical for Rho GEF proteins, the presence of a spectrin repeat suggests that puratrophin-1 could be targeted to the Golgi-apparatus membrane, where it may regulate certain membrane dynamics through modulating actin (Godi et al. 1998; Lemmon et al. 2002). The CRAL/TRIO domain is implicated in the nerve growth factor (NGF) pathway that leads to neurite outgrowth through activating Rho G (Estrach et al. 2002), which indicates that puratrophin-1 may also have a role in cell differentiation signaling through NGF. In the present study, we showed that the Golgi-apparatus membrane protein and spectrin both form aggregation in the Purkinje cells of patient brains, which strongly supports the hypothesis that puratrophin-1 indeed interacts with these essential cytoskeletons. Formation of these aggregations, which seems to be a new phenomenon implicated in pathogenesis of human disease, could be deleterious for cells, since Golgi-apparatus membrane proteins and spectrin are important in maintaining cellular architecture, as noted for autosomal dominant polycystic kidney diseases (Charron et al. 2000). In addition, it also seems rational to speculate that disturbance of puratrophin-1 may affect Purkinje-cell morphology and eventually cause the peculiar Purkinje-cell atrophy that characterizes chromosome 16q22.1–linked ADCA, since Rho GEFs are implicated particularly in neural morphogenesis and connectivity by regulating actin dynamics (Godi et al. 1998).

Finally, the association of progressive hearing impairment in patients with chromosome 16q22.1–linked ADCA may suggest a role of puratrophin-1 in hearing. As far as we were able to examine by auditory tests, 42.8% of study families had hearing impairment. Audiometric configurations showing mid-frequency U-shaped or flat-shaped pattern also suggested that the hearing impairment of these patients was not a simple age-related hearing loss. However, it should be noted

that some families had moderate hearing impairment, whereas other families had only mild hearing impairment, which may indicate the presence of other modifying genetic factors for this phenotype. Further clinical analyses with use of detailed auditory tests are needed to ascertain how strongly hearing impairment is associated with ataxia. If hearing impairment is confirmed as being complicated by chromosome 16q22.1–linked ADCA, puratrophin-1 will be the first deafness/hearing-impairment protein related to Rho GEF. Since mutations in the γ-actin gene (*ACTG1*; DFN20/26) (Zhu et al. 2003), genes coding proteins that interact with actin (e.g., the myosins espin and harmonin), or a gene coding proteins that coordinate actin polymerization (Mburu et al. 2003) are known to cause deafness, it is possible that puratrophin-1 disruption causes hearing impairment by disturbing actin dynamics in the cochlea. In support of this hypothesis, expression of puratrophin-1 was seen in mouse cochlear hair cells, in which actin is also expressed (Mburu et al. 2003). Rho GTPases are also important regulators of actin cytoskeleton in stereocilia development, which is crucial for auditory transduction (Kollmar 2001). We hypothesize that the *puratrophin-1* gene mutation ultimately causes hearing impairment by dysregulation of actin in the cochlea. Further studies, such as targeted disruption of puratrophin-1 in mouse, will be important for clarifying whether puratrophin-1 has a role in hearing.

In summary, we have identified that a single-nucleotide C→T substitution in the 5′ UTR of the gene *puratrophin-1* is strongly associated with chromosome 16q22.1–linked ADCA. If patients with SCA4 are found to harbor mutations in this gene, it would suggest that the chromosome 16q22.1–linked ADCA in Japan is allelic with SCA4. Identification of the mechanism of puratrophin-1 expression, the upstream signaling cascade that activates puratrophin-1, and the actual Rho GTPase activated by puratrophin-1 would be the next key steps for understanding the molecular mechanisms that underlie cellular degeneration of chromosome 16q22.1–linked ADCA and hearing impairment.

Acknowledgments

We thank the doctors who participated in this work by recruiting families with chromosome 16q22.1–linked ADCA: Drs. Hidenao Sasaki, Department of Neurology, Graduate School, Hokkaido University; Masashi Aoki, Department of Neurology, Graduate School, Tohoku University; Yoshihisa Takiyama, Department of Neurology, Jichi Medical School; Kazuo Yoshizawa, National Mito Hospital; Kazuko Mitani and Yu-ichi Fumimura, Department of Neurology, Tokyo Metropolitan Geriatric Hospital; Hirohiko Murakami, Department of Neurology, Tokyo Women's Medical School; Satoshi Orimo, Department of Neurology, Kanto Central Hospital; Souichiro Mochio, Department of Neurology, Jikei Medical School, The Third Hospital; Kunihiro Yoshida, Department of Clinical Genetics, Shinshu University; Isao Sahashi, Fourth Department of Internal Medicine, Aichi Medical University; Masanori Nakagawa, Department of Neurology, Kyoto Prefectural Medical College; Akihumi Goto, Department of Neurology, Nagasaki Medical Center of Neurology; Hideki Kida, Kida Hospital; Eiichiro Uyama, Department of Neurology, Kumamoto University of Medicine; Jun Goto and Shoji Tsuji, Department of Neurology, Graduate School, University of Tokyo; and Miho Murata and Ichiro Kanazawa, National Center of Neurology and Psychiatry, Ministry of Health, Labor and Welfare. For human and mouse control specimens, we also thank Professors Morio Koike, Department of Pathology, and Ken Kitamura, Department of Audio-Vestibular Neuroscience, Graduate School, Tokyo Medical and Dental University. We thank Ms. Iku Sudo and Ms. Minori Kono for technical assistance. We deeply acknowledge Professors Ichiro Kanazawa, Director of National Center of Neurology and Psychiatry, Ministry of Health, Labor and Welfare, and Shoji Tsuji, Department of Neurology, Graduate School, University of Tokyo, for supporting this study. This study was supported by Grant-in-Aids for Scientific Research on Priority Areas—Advanced Brain Science Project—from Ministry of Education, Culture, Sports, Science and Technology, Japan (to K.I. and H.M.), as well as grants from Research on Intractable Disorders (to H.M.) and from Human Genome and Regenerative Medicine, Ministry of Health, Labor and Welfare, Japan (to K.I. and H.M.).

Web Resources

Accession numbers and URLs for data presented herein are as follows:

Celera Discovery System, http://www.celeradiscoverysystem.com/index.cfm (for candidate genes)

Ensembl, http://www.ensembl.org/ (for genetic map, genomic sequences, ESTs, and 21 candidate genes, including *Q9H7K4* and *SLC9A5*)

GenBank, http://www.ncbi.nlm.nih.gov/Genbank/ (for microsatellite DNA markers *GGAA10* [accession number AB13610], TTCC01 [accession number AB13611], *TA001* [accession number AB13612], *GA001* [accession number AB197662], and *AAT01* [accession number AB13613] and full-length and short-form *puratrophin-1* mRNAs [accession numbers AB197663 and AB197664])

NCBI, http://www.ncbi.nlm.nih.gov/ (for DKFZP434I216 [accession numbers BC054486 and AK024475])

Online Mendelian Inheritance in Man (OMIM), http://www.ncbi.nlm.nih.gov/Omim/ (for 16q-linked ADCA type III, or SCA4)

The Hereditary Hearing Loss Homepage, http://webhost.ua.ac.be/hhh/

UniGene, http://www.ncbi.nlm.nih.gov/UniGene/ (for candidate genes and ESTs)

References

Bergeron C, Beric-Maskarel K, Muntasser S, Weyer L, Somerville M, Percy ME (1994) Neurofilament light and polyaden-

ylated mRNA levels are decreased in amyotrophic lateral sclerosis motor neurons. J Neuropathol Exp Neurol 53:221–230

Charron AJ, Bacallao RL, Wandinger-Ness A (2000) ADPKD: a human disease altering Golgi function and basolateral exocytosis in renal epithelia. Traffic 1:675–686

Chen D-H, Brkanac Z, Verlinde CLMJ, Tan X-J, Bylenok L, Nochlin D, Matsushita M, Lipe H, Wolff J, Fernandez M, Cimino PJ, Bird TD, Raskind WH (2003) Missense mutations in the regulatory domain of PKCγ: a new mechanism for dominant nonepisodic cerebellar ataxia. Am J Hum Genet 72:839–849

Estrach S, Schmidt S, Diriong S, Penna A, Blangy A, Fort P, Debant A (2002) The human Rho-GEF trio and its target GTPase RhoG are involved in the NGF pathway, leading to neurite outgrowth. Curr Biol 12:307–312

Flanigan K, Gardner K, Alderson K, Galster B, Otterud B, Leppert MF, Kaplan C, Ptacek LJ (1996) Autosomal dominant spinocerebellar ataxia with sensory axonal neuropathy (SCA4): clinical description and genetic localization to chromosome 16q22.1. Am J Hum Genet 59:392–399

Fucini RV, Navarrete A, Vadakkan C, Lacomis L, Erdjument-Bromage H, Tempst P, Stamnes M (2000) Activated ADP-ribosylation factor assembles distinct pools of actin on Golgi membranes. J Biol Chem 275:18824–18829

Ge WW, Leystra-Lantz C, Wen W, Strong MJ (2003) Selective loss of trans-acting instability determinants of neurofilament mRNA in amyotrophic lateral sclerosis spinal cord. J Biol Chem 278:26558–26563

Godi A, Santone I, Pertile P, Devarajan P, Stabach PR, Morrow JS, DiTullio G, Polishchuk R, Petrucci TC, Luini A, DeMatteis MA (1998) ADP ribosylation factor regulates spectrin binding to the Golgi complex. Proc Natl Acad Sci USA 95: 8607–8612

Graham DI, Lantos PL (eds) (2002) Greenfield's neuropathology, 7th ed. Arnold, London

Hadano S, Hand CK, Osuga H, Yanagisawa Y, Otomo A, Devon RS, Miyamoto N, Showguchi-Miyata J, Okada Y, Singaraja R, Figlewicz DA, Kwiatkowski T, Hosler BA, Sagie T, Skaug J, Nasir J, Brown RH Jr, Scherer SW, Rouleau GA, Hayden MR, Ikeda JE (2001) A gene encoding a putative GTPase regulator is mutated in familial amyotrophic lateral sclerosis 2. Nat Genet 29:166–173

Harding AE (1982) The clinical features and classification of the late onset autosomal dominant cerebellar ataxias: a study of 11 families, including descendants of "Drew family of Walworth." Brain 105:1–28

Hellenbroich Y, Bubel S, Pawlack H, Opitz S, Vieregge P, Schwinger E, Zuhlke C (2003) Refinement of the spinocerebellar ataxia type 4 locus in a large German family and exclusion of CAG repeat expansion in this region. J Neurol 250:668–671

Hirano R, Takashima H, Okubo R, Tajima K, Okamoto Y, Ishida S, Tsuruta K, Arisato T, Arata H, Nakagawa M, Osame M, Arimura K (2004) Fine mapping of 16q-linked autosomal dominant cerebellar ataxia type III in Japanese families. Neurogenetics 5:215–221

Holmes SE, O'Hearn EE, McInnis MG, Gorelick-Feldman DA, Kleiderlein JJ, Callahan C, Kwak NG, Ingersoll-Ashworth RG, Sherr M, Sumner AJ, Sharp AH, Ananth U, Seltzer WK, Boss MA, Vieria-Saecker AM, Epplen JT, Riess O, Ross CA, Margolis RL (1999) Expansion of a novel CAG trinucleotide repeat in the 5′ region of PPP2R2B is associated with SCA12. Nat Genet 23:391–392

Hughes CP, Berg L, Danziger WL, Coben LA, Martin RL (1982) A new clinical scale for the staging of dementia. Br J Psychiatry 140:566–572

Ishikawa K, Fujigasaki H, Saegusa H, Ohwada K, Fujita T, Iwamoto H, Komatsuzaki Y, Toru S, Toriyama H, Watanabe M, Ohkoshi N, Shoji S, Kanazawa I, Tanabe T, Mizusawa H (1999) Abundant expression and cytoplasmic aggregation of α1A voltage-dependent calcium channel protein associated with neurodegeneration in spinocerebellar ataxia type 6. Hum Mol Genet 8:1185–1193

Ishikawa K, Nagaoka U, Takashima M, Yoshizawa K, Yoshizawa T, Ishikawa M, Yamawaki T, Shoji S, Mizusawa H (2000) A gene on SCA4 locus causes dominantly-inherited pure cerebellar ataxia. Neurology 54:1971–1975

Ishikawa K, Tanaka H, Saito M, Ohkoshi N, Fujita T, Yoshizawa K, Ikeuchi T, Watanabe M, Hayashi A, Takiyama Y, Nishizawa M, Nakano I, Matsubayashi K, Miwa M, Shoji S, Kanazawa I, Tsuji S, Mizusawa H (1997) Japanese families with autosomal dominant pure cerebellar ataxia map to chromosome 19p13.1-p13.2 and are strongly associated with mild CAG expansions in the spinocerebellar ataxia type 6 gene in chromosome 19p13.1. Am J Hum Genet 61:336–346

Kobayashi K, Nakahori Y, Miyake M, Matsumura K, Kondo-Iida E, Nomura Y, Segawa M, Yoshioka M, Saito K, Osawa M, Hamano K, Sakakihara Y, Nonaka I, Nakagome Y, Kanazawa I, Nakamura Y, Tokunaga K, Toda T (1998) An ancient retrotransposal insertion causes Fukuyama-type congenital muscular dystrophy. Nature 394:388–392

Koide R, Kobayashi S, Shimohata T, Ikeuchi T, Maruyama M, Saito M, Yamada M, Takahashi H, Tsuji S (1999) A neurological disease caused by an expanded CAG trinucleotide repeat in the TATA-binding protein gene: a new polyglutamine disease? Hum Mol Genet 8:2047–2053

Kollmar R (2001) Who does the hair cell's 'do? Rho GTPases and hair-bundle morphogenesis. Curr Opin Neurobiol 9:394–398

Koob MD, Moseley ML, Schut LJ, Benzow KA, Bird TD, Day JW, Ranum LP (1999) An untranslated CTG expansion causes a novel form of spinocerebellar ataxia (SCA8). Nat Genet 21:379–384

Kutsche K, Yntema H, Brandt A, Jantke I, Nothwang HG, Orth U, Boavida MG, David D, Chelly J, Fryns J-P, Moraine C, Ropers H-H, Hamel BCJ, van Bokhoven H, Gal A (2000) Mutations in *ARHGEF6*, encoding a guanine nucleotide exchange factor for Rho GTPases, in patients with X-linked mental retardation. Nat Genet 26:247–250

Lemmon MA, Ferguson KM, Abrams CS (2002) Pleckstrin homology domains and cytoskeleton. FEBS Lett 513:71–76

Li M, Ishikawa K, Toru S, Tomimitsu H, Takashima M, Goto J, Takiyama Y, Sasaki H, Imoto I, Inazawa J, Toda T, Kanazawa I, Mizusawa H (2003) Physical map and haplotype analysis of 16q-linked autosomal dominant cerebellar ataxia (ADCA) type III in Japan. J Hum Genet 48:111–118

Margolis RL (2002) The spinocerebellar ataxias: order emerges from chaos. Curr Neurol Neurosci Rep 2:447–456

Matsuura T, Yamagata T, Burgess DL, Rasmussen A, Grewal RP, Watase K, Khajavi M, McCall AE, Davis CF, Zu L, Achari M, Pulst SM, Alonso E, Noebels JL, Nelson DL, Zoghbi HY, Ashizawa T (2000) Large expansion of the ATTCT pentanucleotide repeat in spinocerebellar ataxia type 10. Nat Genet 26:191–194

Mburu P, Mustapha M, Varela A, Weil D, El-Amraoui A, Holme RH, Rump A, Hardisty RE, Blanchard S, Coimbra RS, Perfettini I, Parkinson N, Mallon A-M, Glenister P, Rogers MJ, Paige AJ, Moir L, Clay J, Rosenthal A, Liu XZ, Blanco G, Steel KP, Petit C, Brown SDM (2003) Defects in whirlin, a PDZ domain molecule involved in stereocilia elongation, cause deafness in the whirler mouse and families with DFNB31. Nat Genet 34:421–428

Owada K, Ishikawa K, Toru S, Ishida G, Gomyoda M, Tao O, Noguchi Y, Kitamura K, Kondo I, Noguchi E, Arinami T, Mizusawa H. A clinical, genetic and neuropathologic study in a family with 16q-linked ADCA type III. Neurology (in press)

Pasteris NG, Cadle A, Logie LJ, Porteous ME, Schwartz CE, Stevenson RE, Glover TW, Wilroy RS, Gorski JL (1994) Isolation and characterization of the faciogenital dysplasia (Aarskog-Scott syndrome) gene: a putative Rho/Rac guanine nucleotide exchange factor. Cell 79:669–678

Ross CA, Poirier MA (2004) Protein aggregation and neurodegenerative disease. Nat Med Suppl 10:S10–S17

Rossman KL, Der CJ, Sondek J (2005) GEF means go: turning on RHO GTPases with guanine nucleotide-exchange factors. Nat Rev Mol Cell Biol 6:167–180

Sasaki H, Yabe I, Tashiro K (2003) The hereditary spinocerebellar ataxias in Japan. Cytogenet Genome Res 100:198–205

Sgourou A, Routledge S, Antoniou M, Papachatzopoulou A, Psiouri L, Athanassiadou A (2004) Thalassaemia mutations within the 5′ UTR of the human β-globin gene disrupt transcription. Br J Haematol 124:828–835

Stevanin G, Bouslam N, Thobois S, Azzedine H, Ravaux L, Boland A, Schalling M, Broussole E, Durr A, Brice A (2004) Spinocerebellar ataxia with sensory neuropathy (SCA25) maps to chromosome 2p. Ann Neurol 55:97–104

Stevanin G, Durr A, Brice A (2000) Clinical and molecular advances in autosomal dominant cerebellar ataxias: from genotype to phenotype and physiopathology. Eur J Hum Genet 8:4–18

Tsuiki T, Sasamori S, Minami Y, Ichinohe T, Murai K, Murai S, Kawashima H (2002) [Age effect on hearing: a study on Japanese.] Audiol Japan 45:241–250

Tsunemi T, Saegusa H, Ishikawa K, Nagayama S, Murakoshi T, Mizusawa H, Tanabe T (2002) Novel $Ca_v2.1$ splice variants isolated from Purkinje cells do not generate P-type Ca^{2+} current. J Biol Chem 277:7214–7221

van Swieten JC, Brusse E, de Graaf BM, Krieger E, van de Graaf R, de Koning I, Maat-Kievit A, Leegwater P, Dooijes D, Oostra BA, Heutink P (2003) A mutation in the fibroblast growth factor 14 gene is associated with autosomal dominant cerebellar ataxia. Am J Hum Genet 72:191–199 (erratum 72:1078)

Verhoeven K, De Jonghe P, Van de Putte T, Nelis E, Zwijsen A, Verpoorten N, De Vriendt E, Jacobs A, Van Gerwen V, Francis A, Ceuterick C, Huylebroeck D, Timmerman V (2003) Slowed conduction and thin myelination of peripheral nerves associated with mutant Rho guanine-nucleotide exchange factor 10. Am J Hum Genet 73:926–932

Yang Y, Hentati A, Deng HX, Dabbagh O, Sasaki T, Hirano M, Hung WY, Ouahchi K, Yan J, Azim AC, Cole N, Gascon G, Yagmour A, Ben-Hamida M, Pericak-Vance M, Hentati F, Siddique T (2001) The gene encoding alsin, a protein with three guanine-nucleotide exchange factor domains, is mutated in a form of recessive amyotrophic lateral sclerosis. Nat Genet 29:160–165

Yu GY, Howell MJ, Roller MJ, Xie TD, Gomez CM (2005) Spinocerebellar ataxia type 26 maps to chromosome 19p13.3 adjacent to SCA6. Ann Neurol 57:349–354

Zhu M, Yang T, Wei S, DeWan AT, Morell RJ, Elfenbein JL, Fisher RA, Leal SM, Smith RJH, Friderici KH (2003) Mutations in the γ-actin gene (*ACTG1*) are associated with dominant progressive deafness (DFNA20/26). Am J Hum Genet 73:1082–1091

Zhuchenko O, Bailey J, Bonnen P, Ashizawa T, Stockton DW, Amos C, Dobyns WB, Subramony SH, Zoghbi HY, Lee CC (1997) Autosomal dominant cerebellar ataxia (SCA6) associated with small polyglutamine expansions in the α1A-voltage-dependent calcium channel. Nat Genet 15:62–69

A clinical, genetic, and neuropathologic study in a family with 16q-linked ADCA type III

Abstract—Presented is the new kindred with autosomal dominant cerebellar ataxia linked to chromosome 16q22.1 (16q-ADCA type III) associated with progressive hearing loss. By haplotype analysis, the critical interval was slightly narrowed to three megabase regions between GATA01 and D16S3095. Neuropathologic study of 16q-ADCA type III demonstrated characteristic shrinkage of Purkinje cell bodies surrounded by synaptophysin-immunoreactive amorphous material containing calbindin- and ubiquitin-positive granules.

NEUROLOGY 2005;65:629–632

K. Owada, MD, PhD; K. Ishikawa, MD, PhD; S. Toru, MD, PhD; G. Ishida, MD, PhD; M. Gomyoda, MD, PhD; O. Tao, MD; Y. Noguchi, MD, PhD; K. Kitamura, MD, PhD; I. Kondo, MD, PhD; E. Noguchi, MD, PhD; T. Arinami, MD, PhD; and H. Mizusawa, MD, PhD

Autosomal dominant cerebellar ataxia (ADCA) type III is characterized by purely cerebellar ataxia throughout different generations.[1] We previously described families with ADCA type III that map to chromosome 16q13.1-q22.1[2] (16q-ADCA type III; OMIM: %600223), the same region to which maps spinocerebellar ataxia type 4 (SCA4).[3] We subsequently found that families with 16q-ADCA type III harbor a common, 'founder' haplotype for the 3.8 mega-base (Mb) region between GGAA05 and D16S3095.[4]

We describe here the new five-generation kindred with 16q-ADCA type III and slightly narrowed candidate region. We also report the first neuropathologic data of 16q-ADCA type III.

Methods. *Clinical analysis.* The index patient (Patient III-1; figure 1) first consulted our clinic because of unsteadiness of gait. Multiple family members over five generations were documented to have progressive ataxia (see figure 1). Interview and neurologic examination were performed in 12 individuals (Patients II-11, III-1, III-16, III-18, III-20, IV-1, IV-2, IV-3, IV-6, IV-7, V-1, and V-2). Patient II-11 was also examined neuropathologically. This patient presented with gait ataxia at age 70 and experienced hearing difficulties from age 75. Both symptoms slowly progressed. At age 90, she had prominent ataxia and could not walk without assistance. She became bed-ridden at age 92 and died of natural causes at age 96.

Genetic analysis. After obtaining informed consent, genomic DNA was extracted from peripheral blood from 12 individuals (see figure 1). After excluding spinocerebellar ataxia (SCA) 1, 2, 3, 6, 7, 12, and 17 and dentatorubral and pallidoluysian atrophy, genotypes were determined for 12 informative markers on chromosome 16q22.1[4,5] (see table E-1 on the *Neurology* Web site at www.neurology.org). Allele frequencies in general population were analyzed in 50 unrelated individuals without histories of ataxia or other neurodegenerative diseases. Two-point and multipoint lod scores were calculated using software LINKAGE (ver 5.1) and GENEHUNTER.

Neuropathological analysis. The brain and spinal cord were fixed in 10% neutral buffered formalin for two weeks. Paraffin-embedded sections were stained by hematoxylin and eosin (H&E), Klüver-Barrera (KB), and modified Bielschowsky methods. Immunohistochemistry was undertaken using standard avidin-biotinylated peroxidase complex (ABC) method and developed with diaminobenzidine (DAB). Primary antibodies used were mouse monoclonal antibodies against expanded polyglutamine (*1C2*; Chemicon; diluted into 1:4000), calbindin D28k (Sigma; 1:200), synaptophysin (Sigma; 1:50), phosphorylated neurofilament (*SMI31*, Steinberger; 1: 5000), and rabbit polyclonal antibody against ubiquitin (Sigma; 1: 400). Specimens from two individuals, one without neurological diseases and the other with SCA6, served as controls.

Results. *Clinical features.* By neurologic examination, seven individuals were confirmed as having pure cerebellar ataxia (see figure 1). The individual IV-6 was not confirmed "affected" but showed very mild imbalance. Cardinal features in the seven patients were truncal ataxia (100%), limb ataxia (71.4%), cerebellar speech (71.4%), and reduced muscle tonus (57.1%). Tendon reflexes were normal but were reduced at ankles in 28.6% of patients. Gaze nystagmus was not obvious. Only Patient II-11 had mild positional and action tremor in hands. Decreased sensation, absence of tendon reflexes, and Babinski signs, distinctively seen in SCA4 patients,[3,6] were all absent.

The average age at onset of ataxia was 52.1 years, ranging from 8 to 70 years. Patients IV-1 and V-1 documented their ages at onset at younger than 20 years. Phenomenon

Additional material related to this article can be found on the *Neurology* Web site. Go to www.neurology.org and scroll down the Table of Contents for the August 23 issue to find the title link for this article.

From the Departments of Neurology and Neurological Science (Drs. Owada, Ishikawa, Toru, Tao, and Mizusawa), and Otolaryngology (Drs. Y. Noguchi and Kitamura), Graduate School, Tokyo Medical and Dental University, Tokyo, Departments of Neurology (Dr. Ishida) and Clinical Laboratory (Dr. Gomyoda), National Matsue Hospital, Shimane Prefecture, Department of Medical Genetics (Dr. Kondo), Ehime University School of Medicine, Ehime Prefecture, and Department of Medical Genetics (Drs. E. Noguchi and Arinami), Graduate School of Comprehensive Human Sciences, University of Tsukuba, Ibaraki, Japan.

Dr. Owada's current affiliation is Department of Internal Medicine, Aoyama Hospital, 5-53-3 Jingu-mae, Shibuya-ku 150-0001, Tokyo, Japan.

Supported by Grant-in-Aids for Scientific research on Priority Areas, Advanced Brain Science Project, from the Ministry of Education, Culture, Sports, Science, and Technology, Japan (K.I. and H.M.), as well as Grants for Research on Intractable Disorders, Ministry of Health, Labor and Welfare, Japan (H.M.).

Disclosure: The authors report no conflicts of interest.

Received June 26, 2004. Accepted in final form April 18, 2005.

Address correspondence and reprint requests to Dr. H. Mizusawa, Department of Neurology and Neurological Science, Graduate School, Tokyo Medical and Dental University, 1-5-45 Yushima, Bunkyo-ku 113-8519, Tokyo, Japan.

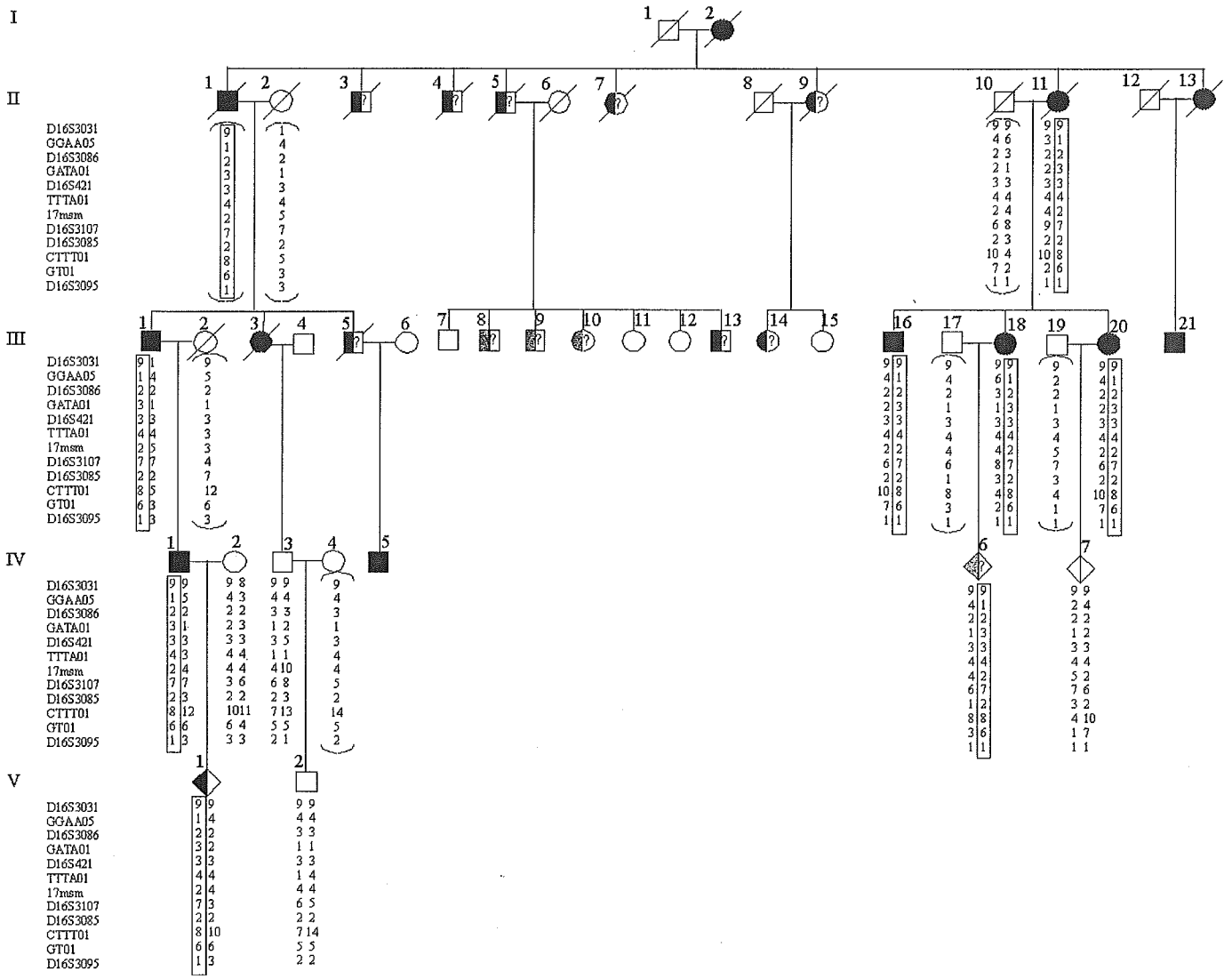

Figure 1. Pedigree of the present family with reconstructed haplotypes for markers at 16q22.1. Women are shown with a circle, and men with a square. Deceased are slashed. Rhombes indicate the sex is not specified because of confidentiality. Individuals with ataxia are filled in the left half of their symbols, and individuals with definite hearing impairment are filled in their right half of their symbols. The individual IV-6 who was suspected of having ataxia was filled gray. The symbol "?" indicates presence of hearing impairment was suspected, but was not confirmed. Individuals III-8, III-9 and III-10 are suspected of having ataxia, since lurching gait and dysarthria have been noticed by several family members. Haplotypes for chromosome 16 markers are shown. The haplotypes cosegrageting with ataxia are boxed. Deduced haplotypes are shown in braces.

of anticipation was generally not obvious but was seen in transmission through Patients III-1, IV-1, and V-1. Brain MRI revealed isolated cerebellar atrophy. Peripheral nerve conduction study and somatosensory evoked potentials in two individuals (Patients III-1 and IV-1) were normal.

Six of seven individuals with ataxia documented hearing difficulties (Patients II-11, III-1, III-16, III-18, III-20, and IV-1). Several other members also seemed to have both ataxia and hearing impairment (I-2, II-1, II-3, III-3, and IV-5). Audiograms, brainstem auditory evoked potentials, and otoacoustic emissions of Patients III-1 and IV-1 indicated that the hearing impairment had a cochlear origin (figure 2). The average age at onset of hearing impairment was 59.4 years.

Genetic features. The highest two-point lod score was obtained with marker CTTT01 with a maximum lod score of 2.2 at $\theta = 0$, supporting linkage to chromosome 16q22.1 (see table E-2). Maximum multipoint lod score reached 2.3, suggesting linkage. Comparing the haplotypes of the current and previous families, different alleles are seen at GATA01: The current family had allele 3, whereas the previous eight families had allele 2[4] (see figure 1; also see table E-1). This would indicate that the gene for with autosomal dominant cerebellar ataxia linked to chromosome 16q22.1 (16q-ADCA type III) lies in the 3-Mb region between GATA01 and D16S3095.

Neuropathologic features. The brain including the brainstem and cerebellum weighed 1,200 g after fixation.

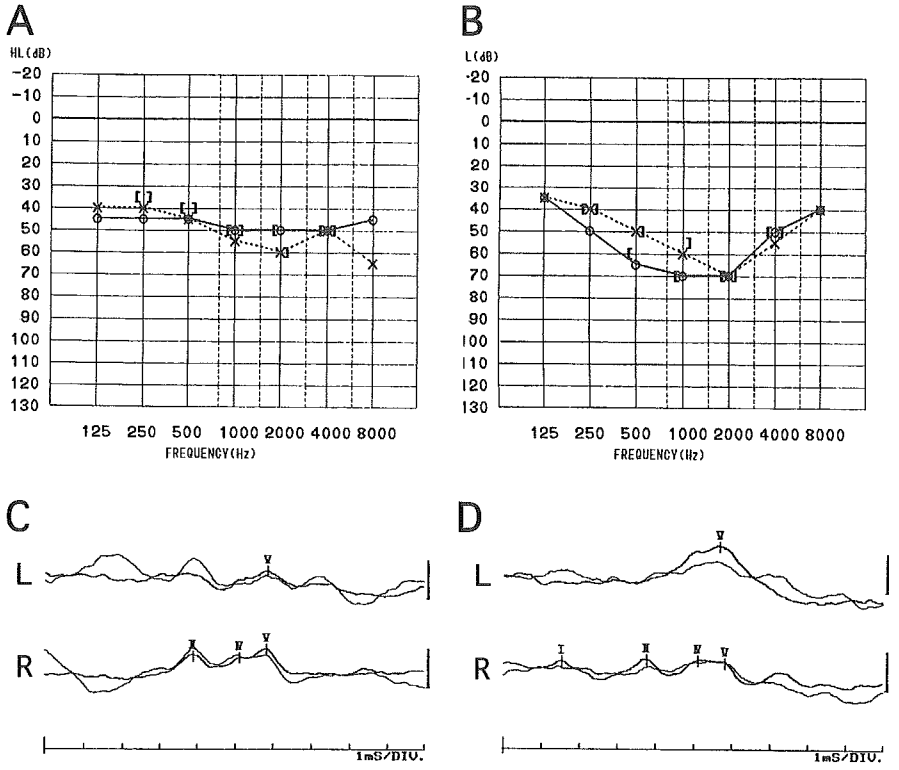

Figure 2. Audiograms of the Patients III-1 (A) and IV-1 (B). Open circle indicates air conduction of the left ear, cross indicates that of the right ear. Symbols [indicate bone conduction of right ear,] indicate that of left ear. Both audiograms show sensorineural hearing impairment, slightly worse in Patient IV-01. BAEPs of the Patients III-1 (C) and IV-1 (D). "L" indicates responses (CZ-A1) elicited by left ear stimulation (90dB, 9.5Hz), and "R" indicates responses (CZ-A2) elicited by right ear stimulation. The BAEPs show poor I-wave formation in both patients, consistent with their internal ear impairments.

Macroscopically, the brain and spinal cord appeared normal except for the moderate cerebellar atrophy in the upper vermis.

Microscopically, the most prominent feature was the Purkinje cell degeneration with relative preservation of molecular and granule cell layers (figure 3A). Generally, the Purkinje cell loss was severe in the anterior lobe such as culmen, moderate in the upper aspect of the posterior lobe, and mild in the rest of the regions such as tonsil. The remaining Purkinje cells were often atrophic and were surrounded by thick amorphous materials (figure 3B). The dentate nucleus had moderate astrogliosis. No obvious pathologic change was seen in the cerebrum, brainstem, including the inferior olivary nucleus or in the spinal cord, although mild myelin pallor was seen in the fasciculus gracilis and the spinocerebellar tracts (figure 3, C and D).

1C2-immunoreactive aggregates were not seen (figure 3E). Ubiquitin-positive granules were seen within the amorphous material, also sometimes within the Purkinje cell body (figure 3F). A few Purkinje cells showed processes stemming from their cell bodies resembling 'somatic sprout' on calbindin D28k immunohistochemistry (figure 3G). Within the amorphous materials, a zone with weak calbindin-immunoreactivity or calbindin-positive granules were seen (figure 3, H and I). The amorphous materials were intensely immunoreactive for synaptophysin (figure 3J), while such finding was not seen in control brains. Immunoreactivity for SMI31 was seen only in the periphery of the amorphous material (figure 3K).

Discussion. We described a new family of 16q-ADCA type III, showing co-segregation of pure cerebellar ataxia and hearing impairment. It is possible that the two phenotypes are caused by a single gene mutation. Since genes for deafness are not known within the candidate region, discovering the 16q-ADCA type III gene would be important. Audiogram and BAEPs are necessary to clarify whether hearing impairment is indeed associated with 16q-ADCA type III.

Neuropathology of 16q-ADCA type III was characterized by shrunken cell bodies, abnormal dendrites, somatic sprouts of Purkinje cells, and the amorphous materials surrounding the Purkinje cell. Although somatic sprouts are described in other diseases such as Menkes' disease,[7] the amorphous materials have not been described.[8] Therefore, presence of amorphous materials around shrunken Purkinje cells could be diagnostic for 16q-ADCA type III. The amorphous materials resemble "grumose degeneration" of the dentate nucleus in DRPLA and progressive supranuclear palsy (PSP).[9] Presence of calbindin- and ubiquitin-immunoreactive granules within the amorphous materials would indicate that the amorphous materials are formed in association both with the degeneration of Purkinje cell processes and the increase of presynaptic terminals innervated either from basket cells, inferior olivary neurons, or other neurons.[10] Alteration of calbindin-immunoreactivity in Purkinje cells may also indicate that the intracellular calcium buffering system, which is one of the important roles of calbindin, may be altered in 16q-ADCA type III.

Note added in proof. After acceptance of this article, a genetic change tightly associated with the 16q-linked ADCA type III including the present family was discovered in the gene encoding a protein with spectrin and Rho guanine-nucleotide exchange-

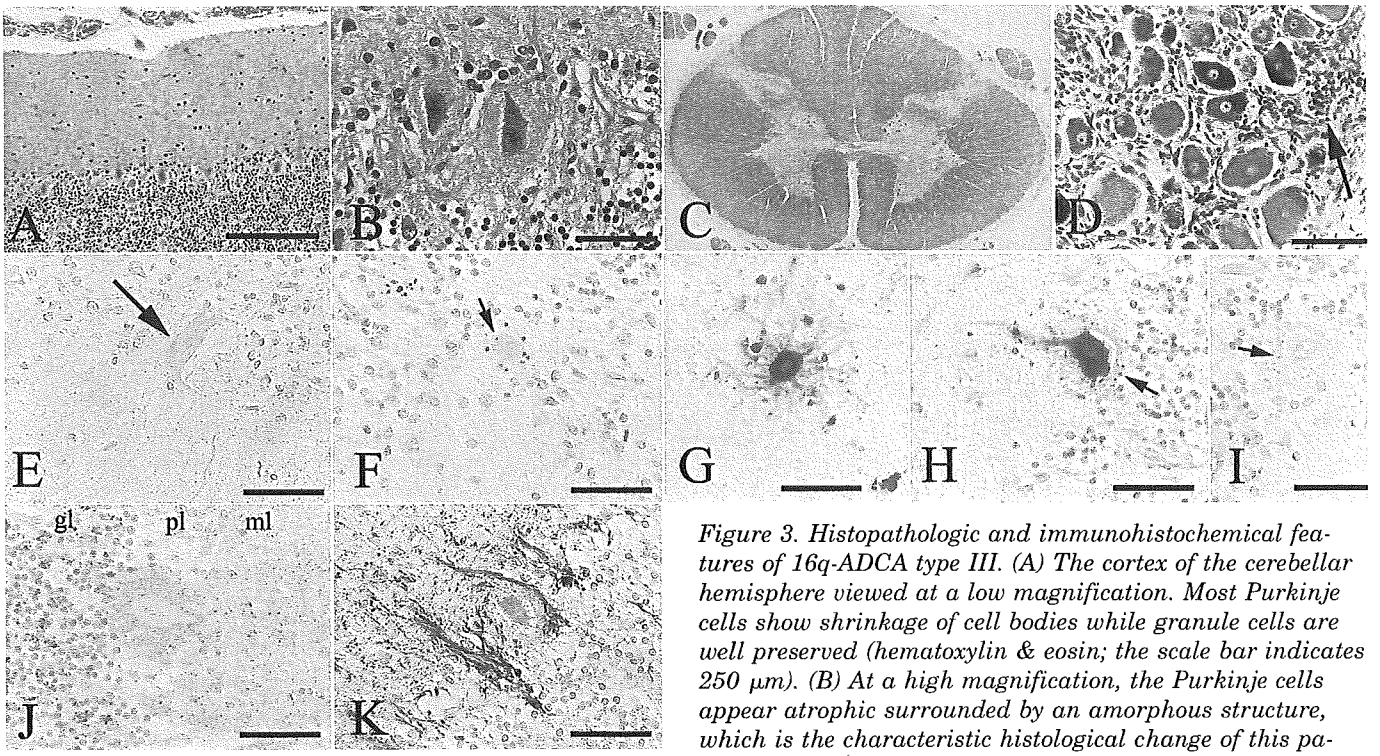

Figure 3. Histopathologic and immunohistochemical features of 16q-ADCA type III. (A) The cortex of the cerebellar hemisphere viewed at a low magnification. Most Purkinje cells show shrinkage of cell bodies while granule cells are well preserved (hematoxylin & eosin; the scale bar indicates 250 μm). (B) At a high magnification, the Purkinje cells appear atrophic surrounded by an amorphous structure, which is the characteristic histological change of this patient (hematoxylin & eosin; the scale bar indicates 50 μm). (C) The thoracic spinal cord. Myelin pallor is seen in the dorsal column and spinocerebellar tracts (Klüver-Barrera staining). (D) The dorsal root ganglia of the 7th thoracic spine. Neuronal loss is not apparent. A Nageotte's nodule is seen (arrow) (Klüver-Barrera staining; the scale bar indicates 10 μm). (E) Immunohistochemistry for expanded polyglutamine using mouse monoclonal antibody 1C2 does not demonstrate microscopic aggregations in the Purkinje cell (arrow) (immunoperoxidase, counter stained with methyl green; scale bar indicates 50 μm). (F) There are some ubiquitin-immunoreactive granules in the amorphous materials. A granule is also seen within the cell body (small arrow) (immunoperoxidase, counter stained with hematoxylin; scale bar indicates 50 μm). (G) Immunohistochemistry for calbindin D28k shows a bizarre-shaped Purkinje cell, called "somatic sprouts" (immunoperoxidase; scale bar indicates 50 μm). (H) A fuzzy and weak immunoreactivity against calbindin D28k is seen at the amorphous structure. Immunoreactive granules are also seen outside the Purkinje cell body (small arrow) (immunoperoxidase, counter stained with hematoxylin; scale bar indicates 50 μm). (I) No obvious immunoreactivity for calbindin is seen in an atrophic Purkinje cell, except for granules within amorphous material (small arrow) (immunoperoxidase, counter stained with hematoxylin; scale bar indicates 50 μm). (J) Synaptophysin immunoreactivity is increased around the Purkinje cell body (pl: Purkinje cell layer). The immunoreactivities at the molecular layer (ml) and at the gromerulus in the granular layer (gl) are not obviously reduced (immunoperoxidase, counter stained with hematoxylin; scale bar indicates 50 μm). (K) The SMI31-immunoreactive basket cell axons attach to the outer margin of the amorphous structure. The Purkinje cell body is weakly immunoreactive for SMI31 (immunoperoxidase, counter stained with methyl green; scale bar indicates 50 μm).

factor domains by the authors (Am J Hum Genet 2005;77:280–296).

Acknowledgment

The authors thank Drs. Jiro Kumagai and Toshihiko Kuroiwa (Department of Pathology, Tokyo Medical and Dental University) for help with the neuropathology and Dr. Hiroto Fujigasaki (Department of Neurology, Tokyo Medical and Dental University) for support.

References

1. Harding AE. The clinical features and classification of the late onset autosomal dominant cerebellar ataxias. A study of 11 families, including descendants of 'Drew family of Walworth'. Brain 1982;105:1–28.
2. Nagaoka U, Takashima M, Ishikawa K, et al. A gene on SCA4 locus causes dominantly-inherited pure cerebellar ataxia. Neurology 2000;54: 1971–1975.
3. Flanigan K, Gardner K, Alderson K, et al. Autosomal dominant spinocerebellar ataxia with sensory axonal neuropathy (SCA4): clinical description and genetic localization to chromosome 16q22.1. Am J Hum Genet 1996;59:392–399.
4. Li M, Ishikawa K, Toru S, et al. Physical map and haplotype analysis of 16q-linked autosomal dominant cerebellar ataxia (ADCA) type III in Japan. J Hum Genet 2003;48:111–118.
5. Hirano R, Takashima H, Okubo R, et al. Fine mapping of 16q-linked autosomal dominant cerebellar ataxia type III in Japanese families. Neurogenetics 2004;5:215–221. Epub 2004 Sep.
6. Hellenbroich Y, Bubel S, Pawlack H, et al. Refinement of the spinocerebellar ataxia type 4 locus in a large German family and exclusion of CAG repeat expansion in this region. J Neurol 2003;250:668–671.
7. Purpura DP, Hirano A, French JH. Polydendritic Purkinje cells in X-linked copper malabsorption: a Golgi study. Brain Res 1976;117:125–129.
8. Koeppen AH, Dickson AC, Lamarche JB, Robitaille Y. Synapses in the hereditary ataxias. J Neuropathol Exp Neurol 1999;58:748–764.
9. Mizusawa H, Yen SH, Hirano A, Llena JF. Pathology of the dentate nucleus in progressive supranuclear palsy: a histological, immunohistochemical and ultrastructural study. Acta Neuropathol 1989;78:419–428.
10. Hamori J, Szentagothai J. Identification under the electron microscope of climbing fibers and their synaptic contacts. Exp Brain Res 1966;1: 65–81.

Acta Neuropathol (2005) 110: 417–425
DOI 10.1007/s00401-005-1066-9

REGULAR PAPER

Masaki Sakamoto · Toshiki Uchihara
Ayako Nakamura · Toshio Mizutani
Hidehiro Mizusawa

Progressive accumulation of ubiquitin and disappearance of α-synuclein epitope in multiple system atrophy-associated glial cytoplasmic inclusions: triple fluorescence study combined with Gallyas-Braak method

Received: 7 December 2004 / Revised: 2 February 2005 / Accepted: 4 July 2005 / Published online: 25 August 2005

Abstract α-Synuclein (αS) and ubiquitin (Ub) are shared constituents of glial cytoplasmic inclusions (GCIs) and Lewy bodies (LBs), both composed of fibrillary structures. Staining profiles of GCIs were investigated with triple immunofluorescence involving immunostaining for αS and Ub, both amplified with catalyzed reporter deposition, and a fluorochrome, thiazin red (TR) that has an affinity to fibrillary structures. After observation for the triple-fluorescent images, the sections were subsequently stained with the Gallyas-Braak method. Sections of putamen, cerebellar white matter and motor cortex from patients suffering from multiple system atrophy (MSA) with varying duration of the disease (4–15 years) were quantified for these staining profiles of Gallyas-positive GCIs. Although most of GCIs were positive for Ub and variably positive for αS, they were consistently negative for TR. The result was opposite in LBs in Lewy body disease with variable affinity to TR, suggesting that the construction of GCIs is different from that of LBs. These four staining features (αS, Ub, TR and Gallyas) alone failed to exhibit apparent correlation with disease duration, lesion site or severity of degeneration as reported previously. The fraction of αS-negative and Ub-positive GCIs, however, linearly increased along the disease progression, while that of αS-positive and Ub-negative GCIs decreased in contrast. This reciprocal change suggests that αS immunoreactivity in GCIs is being replaced by Ub immunoreactivity during the disease progression, which resulted in the ultimate predominance of αS-negative and Ub-positive GCIs in the most advanced case. Interestingly, this predominance of αS-negative and Ub-positive GCIs was a feature of motor cortex, where degeneration usually remains mild in spite of robust appearance of Gallyas-positive GCIs. Another fraction, αS-positive and Ub-positive GCIs were frequent in cerebellar white matter, suggesting that GCI evolution is heterogeneous and dependent also on area examined. Progressive accumulation of Ub with concomitant disappearance of αS epitope and their colocalization, partly shared with LBs, may represent a process of GCI formation, possibly linked to an aspect of degeneration in MSA.

Keywords Triple labeling · CARD · Thiazin red · Confocal laser microscope · Gallyas-Braak

M. Sakamoto
Department of Neurology, Tokyo Metropolitan Neurological Hospital, Tokyo, Japan

M. Sakamoto · T. Uchihara (✉) · A. Nakamura
Department of Neuropathology, Tokyo Metropolitan Institute for Neuroscience, 2-6 Musashi-dai, Fuchu, 183-8526 Tokyo, Japan
E-mail: uchihara@tmin.ac.jp
Tel.: +81-42-3253881
Fax: +81-42-3218678

M. Sakamoto · H. Mizusawa
Department of Neurology and Neurological Science, Tokyo Medical and Dental University, Tokyo, Japan

T. Mizutani
Department of Pathology, Tokyo Metropolitan Neurological Hospital, Tokyo, Japan

Introduction

α-Synuclein (αS) is a major constituent of filamentous inclusion bodies that are pathological hallmarks of a group of adult-onset neurodegenerative disorders designated as synucleinopathies, including Parkinson's disease (PD), dementia with Lewy bodies (DLB), and multiple system atrophy (MSA) [11]. αS is an abundant brain protein primarily expressed in neurons [18], and has a strong tendency to form 10- to 12-nm-sized fibrils in vitro [4, 10, 24], a biophysical property relevant to its role in the pathogenesis of filamentous neural inclusions. In PD and DLB, αS is deposited as Lewy bodies (LBs) or Lewy neurites that accumulate in cell bodies or neuronal processes [2, 16, 31], whereas filamentous aggregates of αS are predominantly found in oligodendrocytes as glial